

Spring 1985

# Digitally implemented Klapper-Kratt FM detector using the Intel-2920 digital signal processor

Chang-Hwan Park

*New Jersey Institute of Technology*

Follow this and additional works at: <https://digitalcommons.njit.edu/theses>



Part of the [Electrical and Electronics Commons](#)

---

## Recommended Citation

Park, Chang-Hwan, "Digitally implemented Klapper-Kratt FM detector using the Intel-2920 digital signal processor" (1985). *Theses*. 1426.

<https://digitalcommons.njit.edu/theses/1426>

This Thesis is brought to you for free and open access by the Theses and Dissertations at Digital Commons @ NJIT. It has been accepted for inclusion in Theses by an authorized administrator of Digital Commons @ NJIT. For more information, please contact [digitalcommons@njit.edu](mailto:digitalcommons@njit.edu).

## **Copyright Warning & Restrictions**

The copyright law of the United States (Title 17, United States Code) governs the making of photocopies or other reproductions of copyrighted material.

Under certain conditions specified in the law, libraries and archives are authorized to furnish a photocopy or other reproduction. One of these specified conditions is that the photocopy or reproduction is not to be “used for any purpose other than private study, scholarship, or research.” If a user makes a request for, or later uses, a photocopy or reproduction for purposes in excess of “fair use” that user may be liable for copyright infringement,

This institution reserves the right to refuse to accept a copying order if, in its judgment, fulfillment of the order would involve violation of copyright law.

**Please Note: The author retains the copyright while the New Jersey Institute of Technology reserves the right to distribute this thesis or dissertation**

Printing note: If you do not wish to print this page, then select “Pages from: first page # to: last page #” on the print dialog screen

The Van Houten library has removed some of the personal information and all signatures from the approval page and biographical sketches of theses and dissertations in order to protect the identity of NJIT graduates and faculty.

DIGITALLY IMPLEMENTED KLAPPER-KRATT FM DETECTOR  
USING THE INTEL-2920 DIGITAL SIGNAL PROCESSOR

BY  
CHANG-HWAN PARK

A THESIS  
SUBMITTED TO THE FACULTY OF  
THE GRADUATE SCHOOL OF  
THE NEW JERSEY INSTITUTE OF TECHNOLOGY  
IN PARTIAL FULFILLMENT OF  
THE REQUIREMENT FOR  
THE DEGREE OF  
MASTER OF SCIENCE IN ELECTRICAL ENGINEERING

1985

Approval of Thesis

Digitally Implemented Klapper-Kratt FM Detector  
Using the INTEL-2920 Digital Signal Processor

by

Chang-Hwan Park

Thesis and Abstract Approved by:

---

Dr. Jacob Klapper

Professor

Electrical Engineering

---

Date

---

---

V I T A

Name in Full : Chang-Hwan Park      Sex : male  
Date of Birth :      Nationality : Korean  
Address :

Degree and Date to be Conferred : BSEE., 1985.

Collegiate Institutions Attended

New Jersey Institute of Technology: Sep. 1983 - May 1985  
Degree: MSEE.      Major : Electrical Engineering  
Date of Degree: May 1985  
Kyungbook National University : Mar. 1974 - Feb. 1978  
Degree: BSEE.      Major : Electrical Engineering  
Date of Degree: Feb. 1978

Publication:      Digitally Implemented Klapper-Kratt FM  
Detector Using the INTEL-2920 DSP.

Positions held : The Ministry of Communications of  
Korean Government, Seoul, Korea.

Career

May 1984 - Aug. 1984 : Worked for the AT & T. Bell Labs.,  
Department of International Networking,  
Holmdel, New Jersey.  
Mar. 1978 - Now : The Ministry of Communications of  
Korean Government  
Mar. 1967 - Apr. 1976 : Worked for the Korea Electric Co.  
Ltd., Maintenance of Power Line Carrier  
& Micro-Wave.

## A B S T R A C T

Title of Thesis: Digitally Implemented Klapper-Kratt FM  
Detector Using the Intel-2920 DSP

Chang-Hwan Park, Master of Science in Elec. Engin., 1985

Thesis directed by: Dr. Jacob Klapper,

Professor of Electrical Engineering

This thesis describes and analyses a digitally implemented FM detector, which is a new member of the family of FM detectors introduced by Drs. Klapper and Kratt.

The properties of the new detector are low delay, excellent sensitivity, extreme linearity, and compatibility of components with integrated circuit technology.

A working model is implemented by adapting FIR digital signal processing methods, and is realized using the Single-Chip Digital Signal Processor INTEL-2920 which is comprised of a micro-processor, scratch-pad data RAMs, program store EPROMs, A/D and D/A conversion circuitry, and I/O circuitry.

The performance of the working model shows very good linearity within its operating range, and in agreement with the earlier derived theory.

## ACKNOWLEDGMENTS

The author gratefully acknowledges the guidance and assistance of his thesis advisor, Dr. Jacob Klapper. He also expresses his appreciation to Dr. J. J. Padalino who have provided experimental materials and Dr. E. Kratt who have advised to prepare this thesis

The author also wishes to express his deep appreciation to his family who have all helped and encouraged to make this work possible.



## TABLE OF CONTENTS

	Page
Chapter 1: Introduction .....	1
References - Chapter 1 .....	9
Chapter 2: Theoretical Analysis.....	11
2.1 Introduction.....	11
2.2 Quasi-Coherent FM Discriminator.....	11
2.3 Cancellation of RF.....	14
2.4 Theoretical Performance.....	15
2.4.1 Modulated Input wave (Narrow-Band).....	15
2.4.2 Modulated Input Wave (Wide-Band).....	16
2.4.3 Sine Wave Interference.....	17
2.4.4 Noise Performance.....	20
References - Chapter 2.....	28
Chapter 3: Implementation.....	30
3.1 Introduction.....	30
3.2 Network Order Evaluation.....	30
3.3 Linearity Realization.....	35
3.4 Algorithm simplification.....	41
3.5 Software Description.....	45
3.6 System Configuration.....	48

CONTENTS (CONTINUED)

3.7	Realization.....	52
	References - Chapter 3.....	54
Chapter 4:	Detector Performance.....	58
4.1	Introduction.....	58
4.2	Narrow Band Performance.....	61
4.3	Wide Band Performance.....	61
	References - Chapter 4.....	65
Chapter 5:	Conclusions.....	69
	References - Chapter 5.....	70
	Bibliography.....	71

CONTENTS (CONTINUED)

LIST OF FIGURES

Figure	Pages
1-1	Block Diagram of the Original Klapper-Kratt Detector.....2
1-2	Output Characteristic of the Original Detector.....4
1-3	Property of Integrator under Wide-Band Condition.....5
1-4	Block Diagram of the First Derivation of the Detector.....6
1-5	Block Diagram of the Second Derivation of the Detector.....7
1-6	Block Diagram of the New Detector.....10
2-1	Output Characteristic of the New Detector.....12
2-2	$\langle e_o(t) \rangle$ vs. $w_f/w_o$ for Various Values of B/A.....18
2-3	Complete Detector for Noise Calculation.....21
2-4	PSD of $x(t)$ and $y(t)$ .....21
2-5	FM Performance.....25
2-6	Threshold Characteristics .....26
3-1	Frequency Response of Differentiators.....32
3-2	Frequency Response of Hilbert Transformers.....33
3-3	Detector Output.....36
3-4	Non-Ideal Block Representations.....37
3-5	Linearity Optimized Detector Output.....40
3-6	Block Diagram of Simplified detector.....42
3-7	Block Diagram of an Equivalent Simplified Detector.....44
3-8	Block Diagram of the Implementation Algorithm.....45
3-9	Block Diagram of the INTEL-2920.....49

CONTENTS (CONTINUED)

3-10	Block Diagram of the System Configuration.....	50
3-11	LPF Characteristics of INTEL-2912.....	51
3-12	Real-Time Program, FMDET2920.KRT.....	55
4-1	Actual Response of the Detector.....	59
4-2	Repetition Property of the Detector.....	50
4-3	Detector Input Wave-Form for the Narrow-Band Performance.....	62
4-4	Detector Response for the Narrow-Band FM.....	63
4-5	Detector Response for the System Delay.....	66
4-6	Wide-Band Performance.....	67

LIST OF TABLES

Table	Page	
2-1	Sine-Wave Interference.....	22
3-1	Detector Coefficients ( Before Optimized ).....	34
3-2	Optimized Detector Coefficients ( Impulse Response ).....	39

# CHAPTER I

## INTRODUCTION

The digitally implemented FM detector described in this paper is a new member of the family of FM detectors, introduced by Drs. Klapper and Kratt, that discriminates a frequency modulated signal with extremely low delay and excellent sensitivity (refs. 1, 2 and 3).

All conventional FM detectors use low-pass filters to remove the undesirable carrier frequency and their harmonics generated in the detection process, and usually a tuned circuit for the FM to AM conversion. These components would normally not be a low delay circuit. However, the components used in the Klapper-Kratt detector, such as integrators, differentiators, summers, and multipliers are low delay elements. Even previous FM detectors using integrators and differentiators for FM to AM conversion, still incorporate low-pass filters in their output circuitry (refs. 4 and 5).

To solve the delay problems of the output circuit, a synchronous demodulator was constructed to detect the amplitude modulated signal. The synchronous demodulator has theoretically zero delay, but has an undesirable product, namely the second harmonic of carrier frequency, which can be eliminated by an additional integrator and multiplier to generate a cancelling signal.

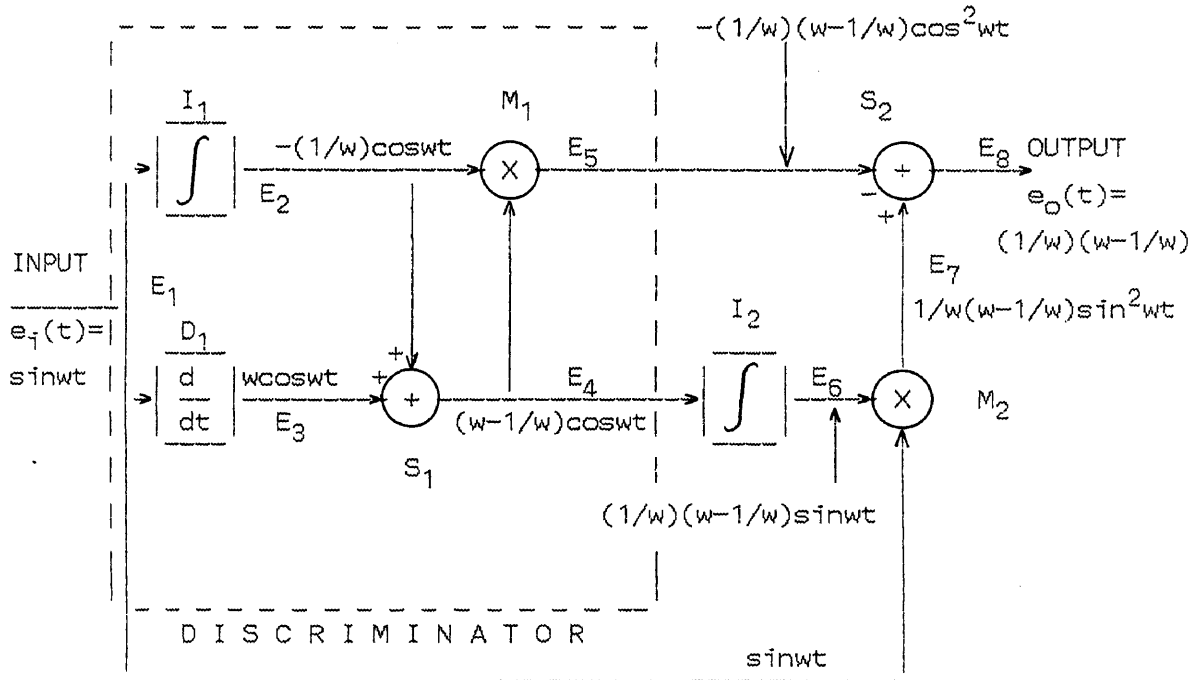


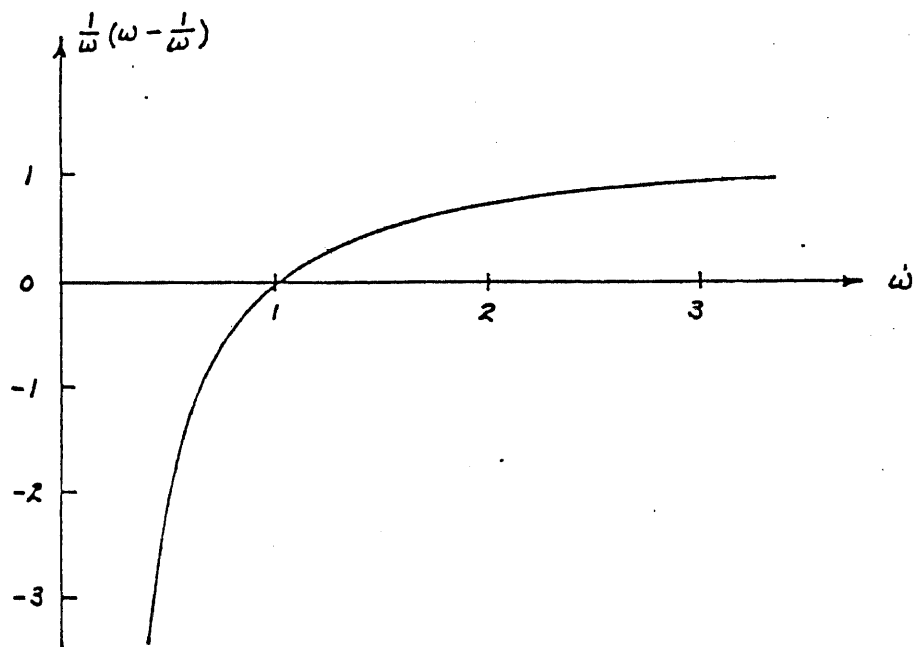
Figure 1-1. Block Diagram of the Original Klapper-Kratt Detector

The original Klapper-Kratt detector is shown in Figure 1-1. The detector performs well under narrow-band conditions, however, there are some undesirable effects when used under wide-band conditions. These are the non-linearity of output characteristics, and DC offset of integrator output when the input frequency changes instantaneously.

The non-linearity of the output causes distortions that are no longer negligible, as indicated in Fig. 1-2. And the DC components of the integrator output, due to the effective initial condition of the integrator at the time of frequency change as shown in Figure 1-3, cause a considerable component of the fundamental carrier frequency to appear at the output of the multiplier.

Another version of detector that does not require integrators in the discrimination section and is not subject to the initial condition is shown in Figure 1-4. Still an integrator is used in the carrier cancellation section, and the output is still non-linear. One more basic form of the Klapper-Kratt detector is shown in Figure 1-5. However, all these versions require integrators and produce outputs that are not ideally linear.

All above mentioned Klapper-Kratt detectors are assumed to be realized by analog means, using operational amplifiers and analog multipliers.



The detector operates at the vicinity of normalized frequency  $\omega = 1$ .

Figure 1-2. Output Characteristic of the Original Detector



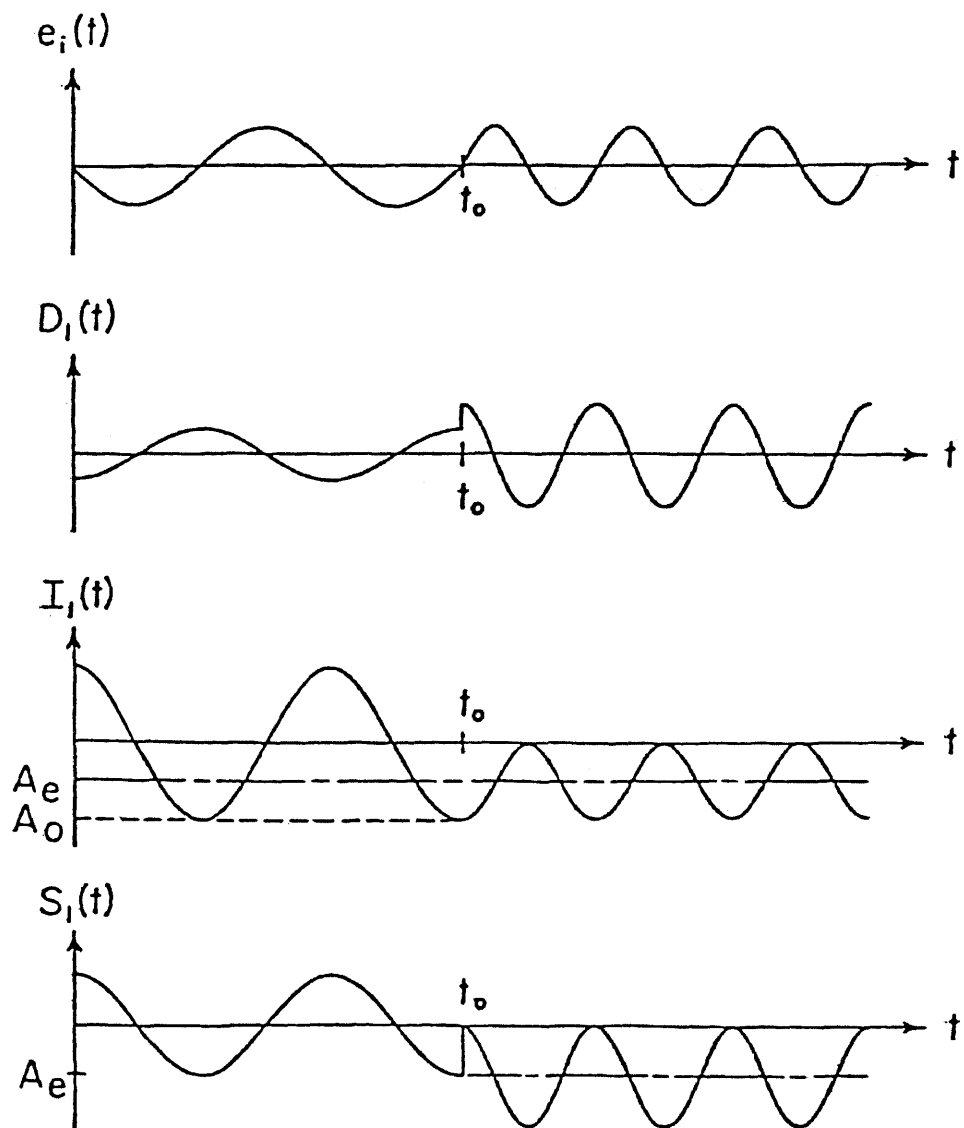


Figure 1-3. Property of the Integrator under Wide-Band Condition

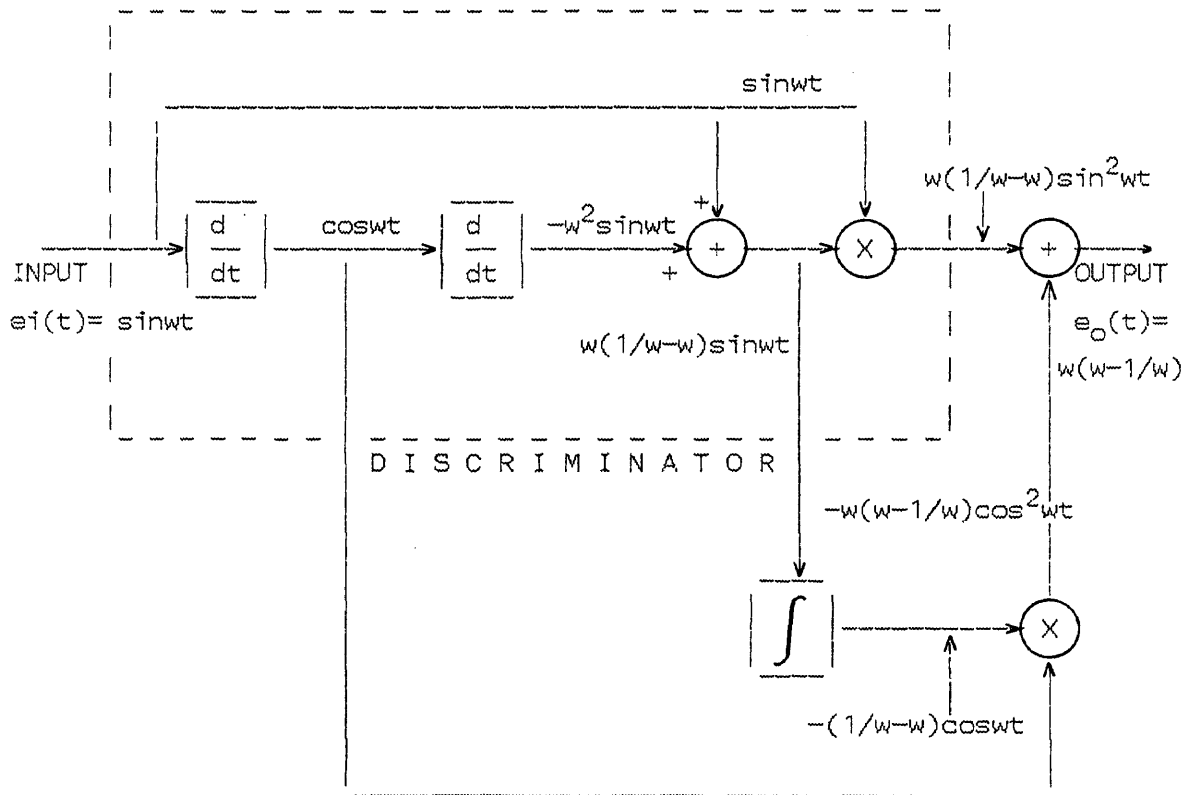


Figure 1-4.

A Block Diagram of

The First Derivation of the Detector

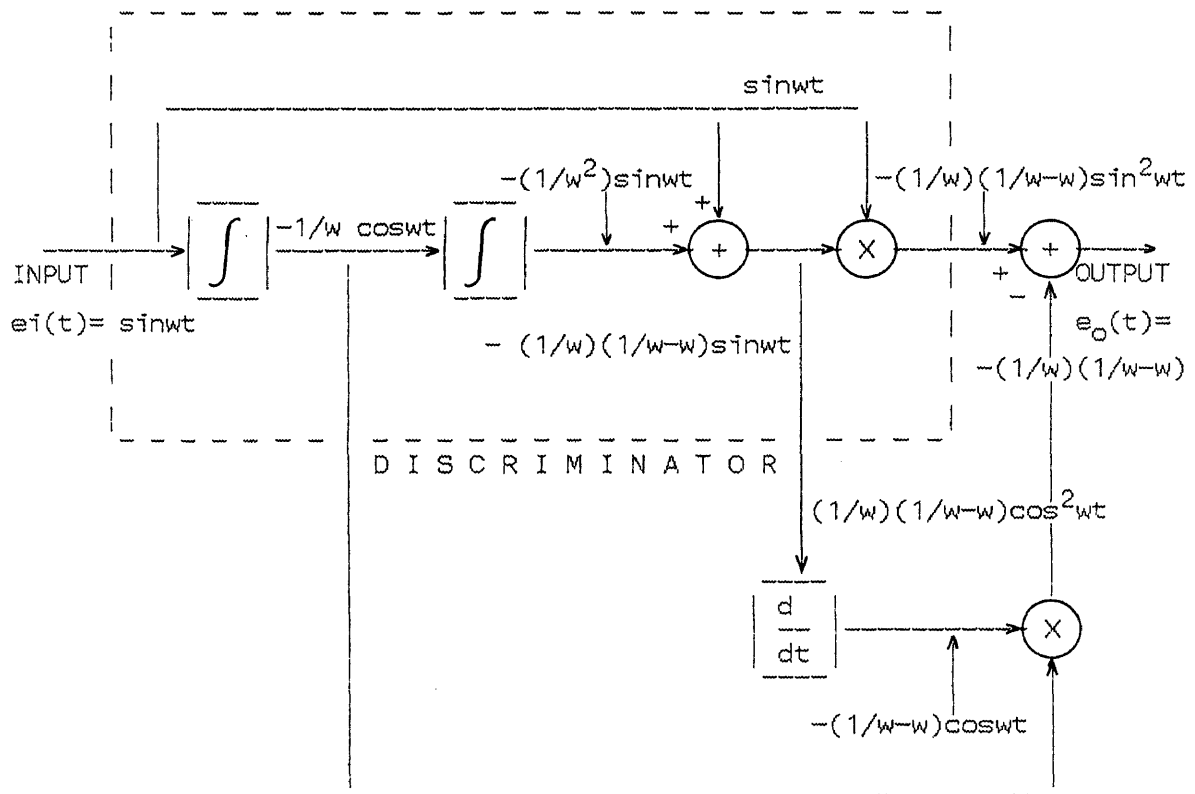


Figure 1-5. A Block Diagram of  
The Second Derivation of the Detector

With the advancement of digital signal processing techniques, an investigation was made to implement the detector by means of digital signal processing techniques.

From the building blocks of the original detector, it was found that the differentiator and multiplier could be realized, but it is preferable to replace the integrator by a Hilbert transformer. The analog realization of a Hilbert transformer is rather complex.

The new detector, adapting Hilbert transformer instead of integrators in Figure 1-1, is given in Figure 1-6 which shows a theoretically perfect linearity and excellent wide-band response. This thesis will mainly be devoted to reveal the characteristics of the new detector.

Chapter 2. will describe theoretical performance, Chapter 3. the digital implementation, Chapter 4. the actual performance of laboratory model and Chapter 5. conclusions

REFERENCES - Chapter 1

1. E. Kratt and J. Klapper, "A New Digital Detector for Frequency Modulated Waves," 27<sup>th</sup> Midwest Symposium on Circuits and Systems, Morgantown, WV, June 1984.
2. E. Kratt, "Optimization of a New Linear FM Detector Using Digital Signal Processing Techniques," A Doctoral Dissertation, NJIT, October 1982.
3. J. Klapper and E. Kratt, "A New Family of Low-Delay FM Detectors," IEEE Transactions on Communications, Vol. COM-27, No. 2, Feb. 1979.
4. J. Park, "An FM Detector for Low S/N," IEEE Transactions on Communication Technology, Vol. COM-18, No. 2, April 1970.
5. K. K. Clarke and D. T. Hess, "Communications Circuits: Analysis and Design," Addison-Wesley, 1971.

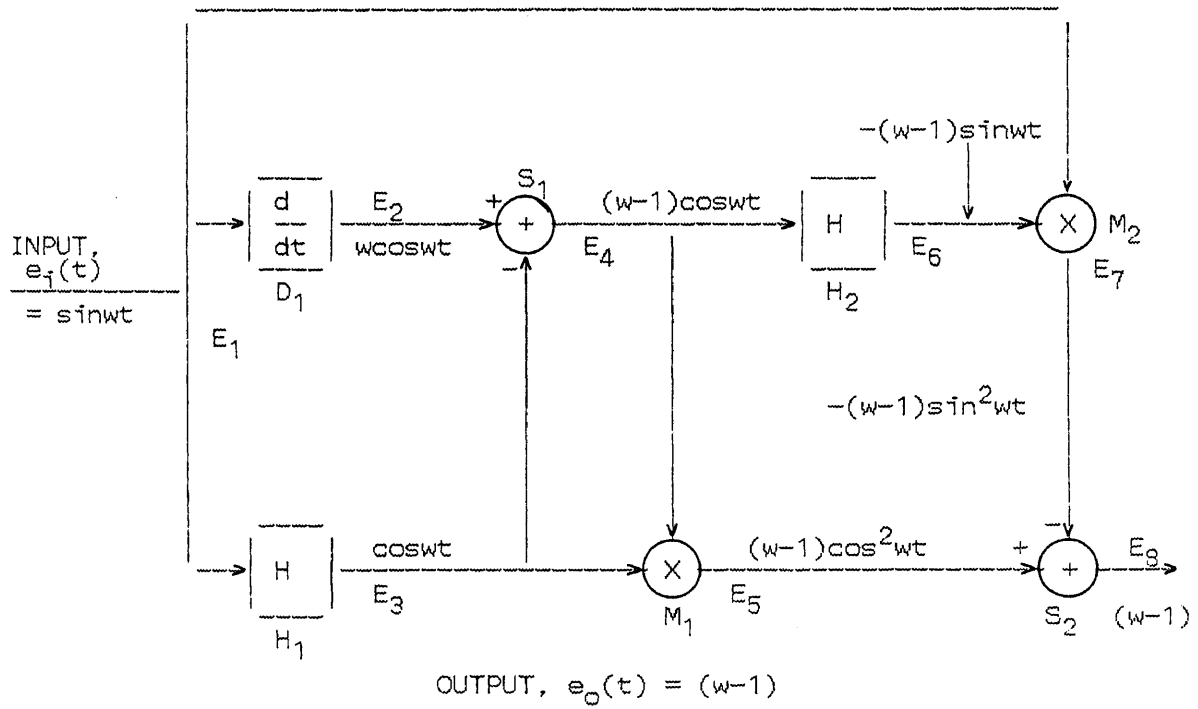


Figure 1-6. Block Diagram of the New Detector .

## CHAPTER II . THEORETICAL ANALYSIS

### 2.1 Introduction

The new detector shown in Figure 1-6 whose output characteristic is shown in Figure 2-1, is comprised of a differentiator, two Hilbert transformers, two multipliers, and two summers. All the components are compatible with digital signal processing methods.

For the analysis of the new detector, we may divide it into two functional blocks, which are 1) wide-band quasi-coherent discriminator, and 2) R-F carrier cancellation.

The theoretical performances of the new detector are also discussed in this chapter under the conditions of 1) modulated input wave, 2) sine-wave interference and 3) noise performance.

### 2.2 Wide-Band Quasi-Coherent FM Discriminator

The FM discrimination is performed by the circuits inside of the dashed box, which are comprised of one differentiator, one Hilbert transformer, one summer, and one multiplier. The differentiator ( $D_1$ ) and the Hilbert transformer ( $H_1$ ) are inputted simultaneously from the input terminal.

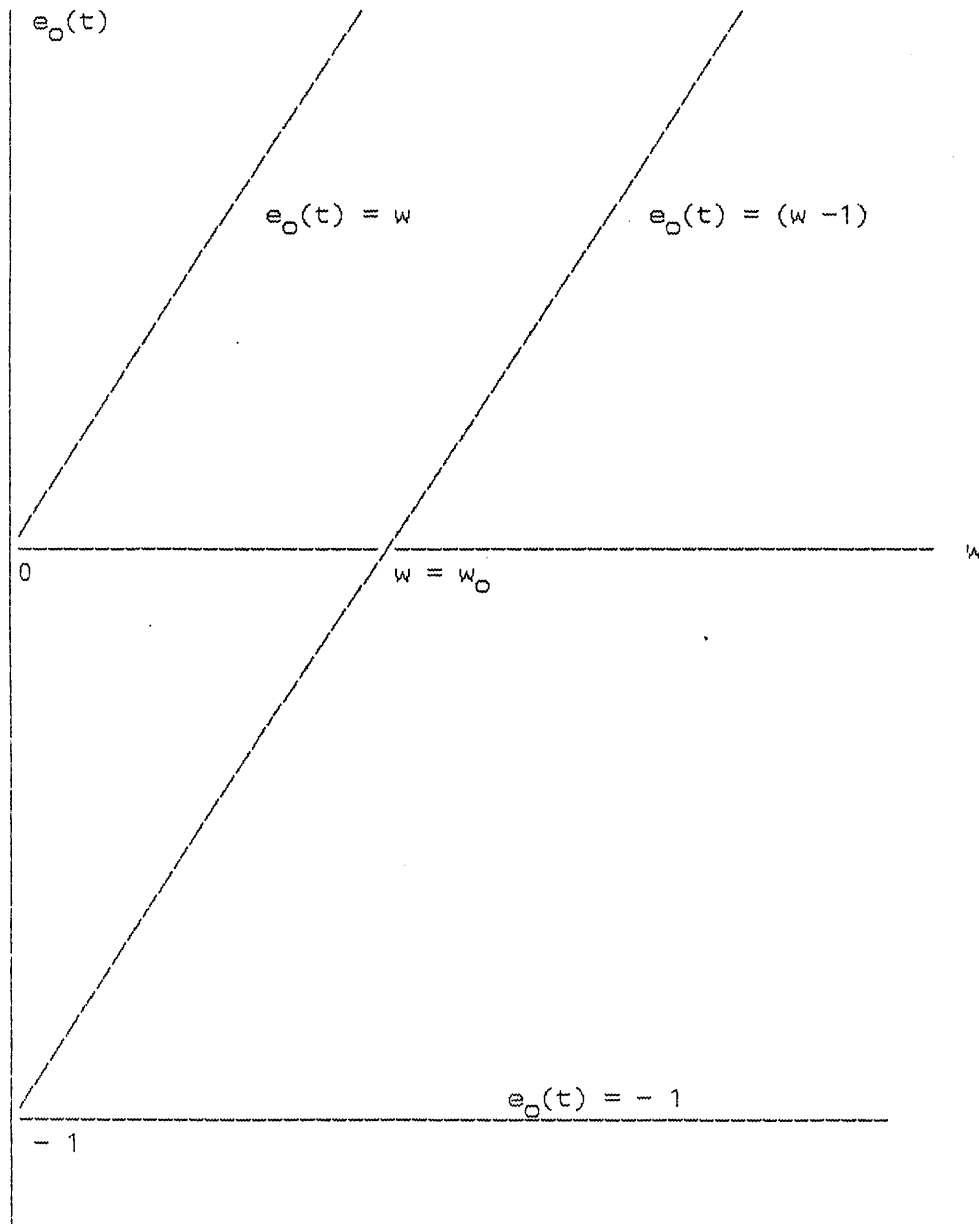


Figure 2-1: Output Characteristic of the  
New Detector



The output amplitude of  $D_1$  varies directly with the input frequency  $w$  and has unit amplitude at  $w = w_0$ , and its phase leads input-wave by 90 degrees, where  $w_0 =$  carrier frequency (or center frequency). The transfer function of  $D_1$ ,  $H_d(f)$ , may be written as

$$H_d(f) = j 2 \pi f, \quad (2-1)$$

The output of the  $H_1$  has a constant amplitude over all the input frequency range, though its phase leads the input by 90 degrees, same as the differentiator, where the transfer function of the digitally implemented Hilbert transformer is inverted from the original one for the ease of implementation. The result is that the outputs of  $D_1$  and  $H_1$  are always in phase. The transfer function of  $H_1$ ,  $H_q(f)$ , may then be written as

$$H_q(f) = j \operatorname{sgn}(f) \quad (2-2)$$

where the  $\operatorname{sgn}(f)$  is a signum function of frequency  $f$ .

The output of the summer( $S_1$ ), which subtracts the output of the  $H_1$  from the  $D_1$ , has the balanced output at  $w = w_0$ , and above and below  $w_0$  it has proportionally increasing amplitude with the frequency difference between input frequency  $w$  and carrier frequency  $w_0$ .

There is a phase reversal, however, when going through  $\omega_0$ , because below  $\omega_0$  Hilbert transformer output dominates and above  $\omega_0$  differentiator output dominates.

The coherent detection is performed by the multiplier  $M_1$ . The inputs of  $M_1$  are one from the output of  $S_1$  and the other from the output of  $H_1$ . The output wave of the multiplier is the FM discriminator output, which contains the demodulated output with the carrier of twice the frequency and modulation index.

The output of the discriminator consists of a dc component and a second harmonic of the carrier, both of which are proportional to  $(w - 1)$ , where the input frequency  $w$  is normalized respect to carrier frequency  $w = \omega_0$ . The output shows a perfect arithmetic symmetry with respect to the center frequency, a property which the other discriminators in the same family can only approximate. Also, all of the components in Figure 1-6 are capable of very wide-band operation and are instantaneous (i.e., introduce no group delay).

### 2.3 Cancellation of RF

The output of  $M_1$ ,  $(w-1)\cos^2 wt$ , is proportional to  $\cos^2 wt$ . And the output of  $M_2$  is proportional to  $\sin^2 wt$ , and its proportionality factor is the same as for  $M_1$ . Then the summer  $S_2$ , which adds the outputs of  $M_1$  and  $M_2$ , cancels the RF carrier frequency.

The inputs of  $S_2$  are  $(w-1)\cos^2 wt$  and  $(w-1)\sin^2 wt$  and the output is only  $(w-1)$ , since  $\cos^2 wt + \sin^2 wt = 1$ . As is shown, the RF cancellation is instantaneous without introducing any delay. This characteristic holds for a modulated input wave because its linearity is perfect. In case of previous versions, however, the RF cancellation is not perfect, due to their non-linearity.

## 2.4 THEORETICAL PERFORMANCE

### 2.4.1 Modulated input wave(Narrow-Band FM)

Consider a narrow-band FM wave, which is a frequency modulated sine-wave with very small modulation index or with a FM wave passed through a narrow-band filter that attenuates all side bands except the first pair, is appearing at the input terminal of Figure 1-6 as  $e_i(t)$ . Then it may be written as

$$e_i(t) = A\{\cos w_o t - (\beta/2)[\cos(w_o - w_m)t - \cos(w_o + w_m)t]\} \quad (2-3)$$

where  $A$  is the amplitude of the wave and  $b$  is the modulation index ( $\beta = \Delta w/w_m$ ), while  $w_o$  and  $w_m$  are the center and modulating frequencies, respectively.

The output of the detector may be derived (Ref. 1) as given by

$$e_o(t) = (A^2 \beta R/2) \cos w_m t = (A^2/2) (\omega/w_o) \cos w_m t \quad (2-4)$$

where  $R = \omega_m/\omega_o$ , is the ratio of the modulating frequency to the center frequency. This equation consists only of a undistorted base-band which is multiplied with a constant.

#### 2.4.2 Theoretical Performance (Wide-Band FM)

A consideration will now be given to the performance of the detector with wide-band modulated input signals, where the input frequency to the detector could change instantaneously.

If the detector is to perform well under the wide-band FM signals, the input of multipliers should not have any dc components. When this condition is violated, a considerable fundamental frequency components will appear at the output. By investigating the inputs of multipliers, no components produce any dc terms under these conditions theoretically ( Ref.1 ).

The new detector should therefore perform equally as well under wide-band conditions. However, this does not hold for other versions of detectors that use integrators, since dc components are generated as a result of the effective initial conditions of the integrators at the time of a rapid frequency change (Figure 1-3).

### 2.4.3 Sine Wave Interference

Consider the case where the input wave consists of a desired frequency  $f_d$  and an interference frequency  $f_i$ , such as

$$e_i(t) = A \cos w_d t + B \cos w_i t \quad (2-5)$$

where  $w = 2\pi f$  and  $w_d = w_o + \Delta w_d$ ,  $w_i = w_o + \Delta w_i$ , and  $f_o$  is the center frequency.

The base-band output of the detector shown in Figure 1-6 is then given by

$$e_o(t) = A^2 (\Delta w_d / w_o) + B^2 (\Delta w_i / w_o) + AB (\Delta w_d / w_o + \Delta w_i / w_o) \cos(w_d - w_i)t \quad (2-6)$$

For the case where  $\Delta f_d = 0$ , which is the carrier frequency without frequency deviation, the normalized output of the detector reduces to

$$e_o(t) = (\Delta w_i / w_o)(B/A)^2 + (\Delta w_i / w_o)(B/A) \cos \Delta w_i t \quad (2-7)$$

and the rms value of the normalized output is given by

$$\langle e_o(t) \rangle = \{ [(\Delta w_i / w_o)(B/A)]^2 + (1/2)[(\Delta w_i / w_o)(B/A)]^2 \}^{1/2} \quad (2-8)$$

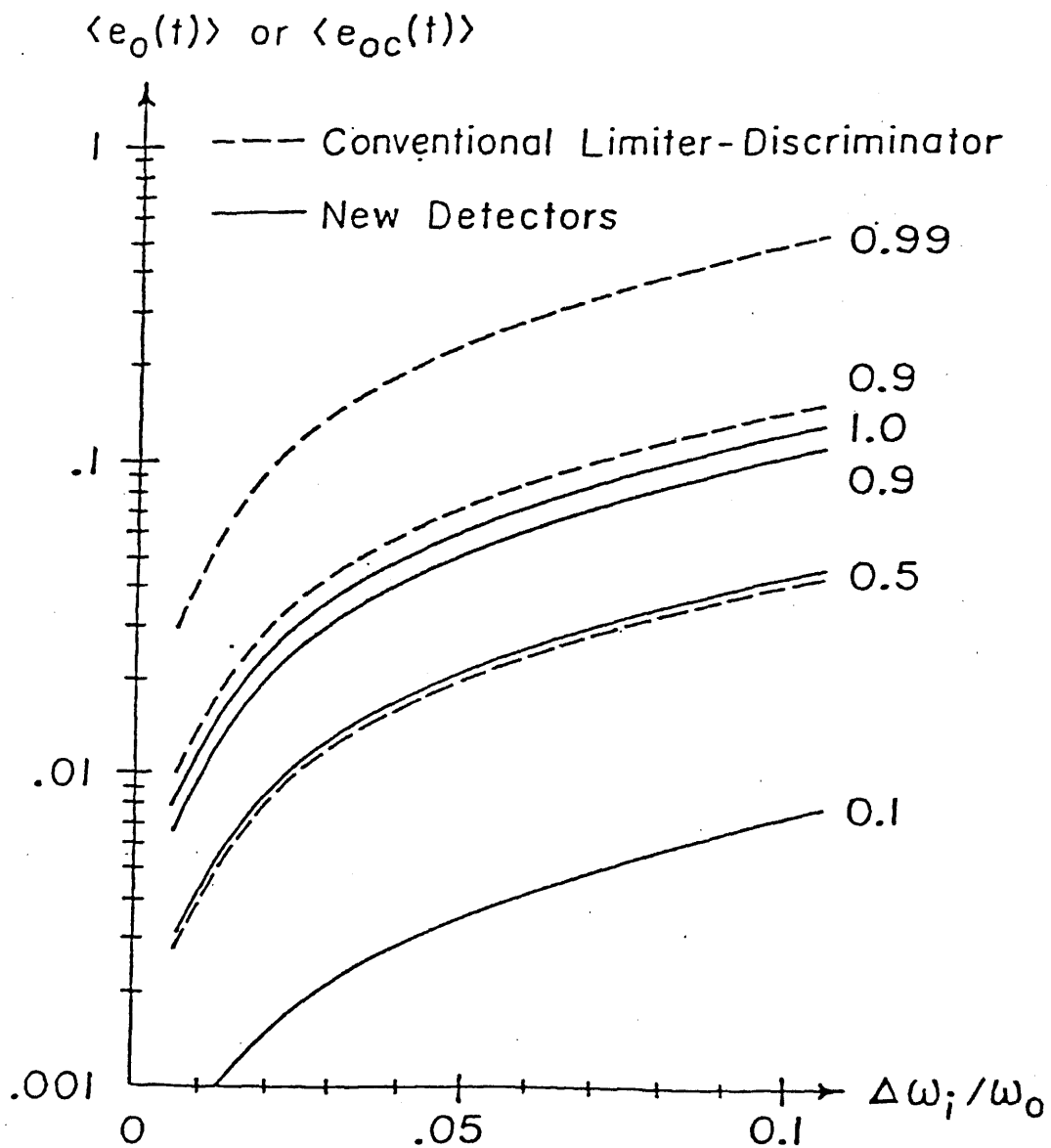


Figure 2-2.  $\langle e_o(t) \rangle$  vs.  $\Delta\omega_i/\omega_o$   
for the various Values of B/A

Curves of  $\langle e_o(t) \rangle$  for the various values of  $B/A$  and  $\Delta w_i/w_o$ , where  $w = 2\pi f$ , are shown in Figure 2-2. Since the output is symmetric about  $\Delta w_i/w_o = 0$ , only positive values of  $\Delta w_i/w_o$  are graphed. For comparison of this result with the conventional wide-band limiter-discriminator case, Corrington (Ref.2) has derived the equivalent output of a conventional wide-band limiter-discriminator for  $\Delta f_d = 0$  as

$$e_{oc}(t) = \frac{(\Delta w_i/w_o)(\cos \Delta w_i t + B/A)}{2 \cos \Delta w_i t + A/B + B/A} \quad (2-9)$$

And the equivalent rms output for  $A/B < 1$  is given by

$$\langle e_{oc}(t) \rangle = \frac{(\Delta w_i/w_o)^2 (B/A)^2}{2[1 - (B/A)^2]} \quad (2-10)$$

The curves of  $\langle e_{oc}(t) \rangle$  for the various values of  $B/A$  and  $\Delta w_i/w_o$  are also shown in Figure 2-2 with dashed curves.

Comparing these curves of Figure 2-2, one observes that the two curves are almost identical for the small values of  $B/A$ . However, as  $B/A$  approaches 1, the output of the ideal limiter-discriminator approaches infinity, while the new detector remains finite. This may be observed by comparing Equation 2-7 and Equation 2-9. Therefore, as the interference increases, the new detector of Figure 1-6 has

a much better output purity both in terms of rms and peak-to-peak values, and this improvement increases without bound. In comparison, similar results for the detectors of the Figures 1-1 and 1-4 as given in the References 3 and 4, respectively, are shown in Table 2-2. The expressions for  $\langle e_o(t) \rangle$  are identical to Equation 2-8 if the frequency deviations are small compared to the carrier frequency ( $\Delta w_i/w_o \ll 1$  and  $\Delta w_d/w_o \ll 1$ ). These assumptions were not needed in the derivation of Equation 2-8, which therefore also describes under the wide-band sinusoidal interference conditions of the new detector

#### 2.4.4 Noise Performance

Referencing to Kratt (Ref. 1), the performance of the new detector in the presence of narrow-band noise will be given. The complete detector, including the pre-detection and post-detection filters, is shown in Figure 2-3. The definition of output SNR used in this derivation is taken to be the ratio of mean output signal power measured in the absence of noise and the noise power taken in the absence of signal, i.e., the carrier is unmodulated. This postulation is valid for high SNR, where the mean signal and noise powers may be assumed to add linearly, and signal power measured in the absence of noise does not differ substantially from that measured with noise present.



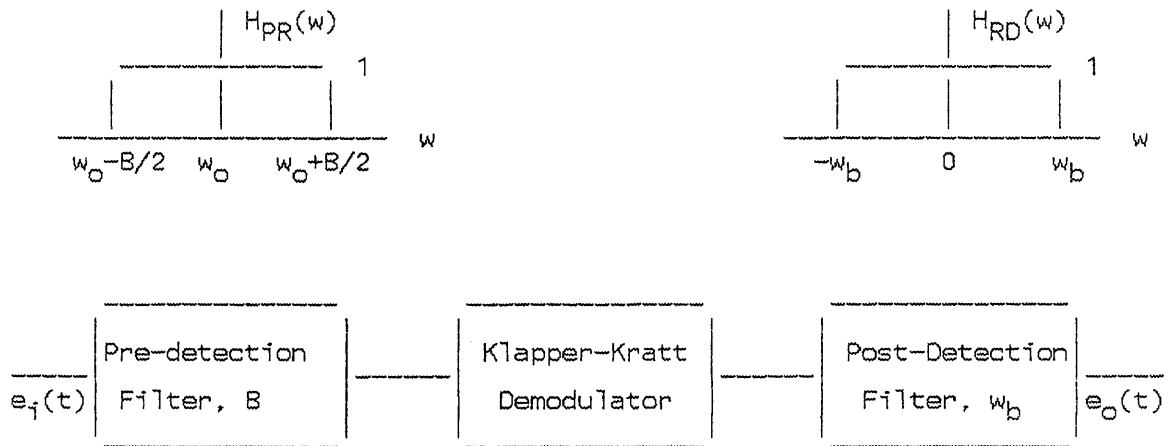


Figure 2-3. Complete Detector for Noise Calculation

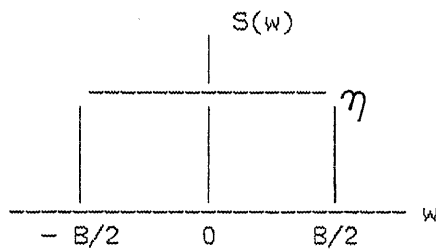


Figure 2-4. PSD OF  $x(t)$  and  $y(t)$

Table 2-1  
Sine Wave Interference

Detector	Normalized $e_o(t)$	$\langle e_o(t) \rangle$	Assumptions
Integrator- Differentiator	$(w_r/w_o)(B/A)^2 +$ $(w_r/w_o)(B/A)\cos w_r t$	$\{U^2 + (1/2) V^2\}^{1/2}$ where, $U = [w_r/w_o (B/A)^2]$ $V = [w_r/w_o B/A]$	$(w_r/w_o) \ll 1$
Dual Differentiator	$-(w_r/w_o)(B/A)^2 -$ $(w_r/w_o)(B/A)\cos w_r t$		$(w_r/w_o) \ll 1$
Differentiator Hilbert Transf	$(w_r/w_o)(B/A) +$ $(w_r/w_o)(B/A)\cos w_r t$		None
Limiter- Discriminator (Conrington)	$\frac{w_r/w_o (\cos w_r t + B/A)}{2\cos w_r t + A/B + B/A}$	$\left[ \frac{(w_r/w_o)^2 (B/A)^2}{2[1 - (B/A)^2]} \right]^{1/2}$	

where  $w_r = \Delta w_d$  for the Dual - Differentiator  
 $= \Delta w_i$  for the others

The signal suppression occurs as the values of CNR drop below 0 dB (Ref. 3).

The noise is assumed to have a bandwidth of no wider than twice the carrier center frequency, and then it may be represented by

$$n(t) = x(t) \cos 2\pi f_0 t - y(t) \sin 2\pi f_0 t \quad (2-11)$$

which consists of the carrier of the center frequency  $f_0$ , modulated by two random variables,  $x(t)$  and  $y(t)$ . The noise is also assumed to be a zero mean Gaussian random variable. The random variables  $x(t)$  and  $y(t)$  thus have the following properties: 1) Low-pass, rectangular power spectral density (PSD) of the bandwidth  $B/2$  and the amplitude  $\eta$  as shown in Figure 2-3 b), 2) Equal variance for  $n(t)$ ,  $x(t)$  and  $y(t)$ , and 3)  $x(t)$  and  $y(t)$  are independent.

Now then, consider an input given by

$$e_i(t) = A \cos 2\pi f_0 t + x(t) \cos 2\pi f_0 t - y(t) \sin 2\pi f_0 t \quad (2-12)$$

which consists of an unmodulated carrier with narrow-band noise added. The baseband output of the detector will then be given by

$$e_o(t) = (1/w_0) \{ x(t)[A - y(t)] + y(t)x(t) \} \quad (2-13)$$

The output PSD of  $e_o(t)$  may then be obtained by taking the Fourier Transform of the autocorrelation of  $e_o(t)$ .

By integrating this result over the post-discrimination bandwidth and dividing by  $2\pi$ , the detector output noise power will then be given by

$$\begin{aligned} \text{NOISE POWER} &= (A^2 \eta w_b^3 / 3\pi w_o^2) \\ &+ (\eta^2 / \pi^2 w_o^2) (B^3 w_b / 12 - B^2 w_b^2 / 8 + B w_b^3 / 6 - w_b^4 / 12) \end{aligned} \quad (2-14)$$

Next, the output signal power may be obtained using a modulated input signal given by

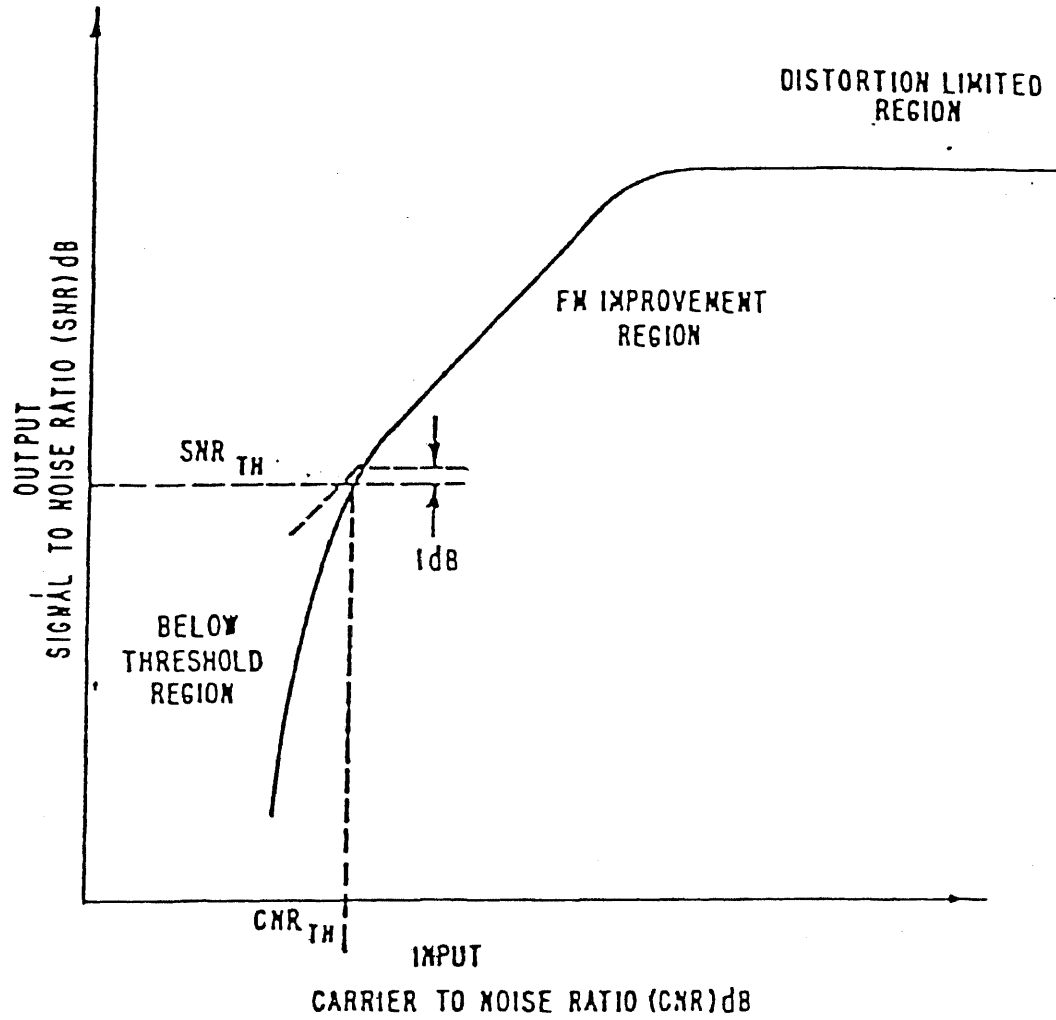
$$e_i(t) = A \cos(w_o t + \beta \sin w_m t) \quad (2-15)$$

where  $A$  is the carrier amplitude,  $\beta$  is the modulation index, and  $w_m$  is the modulation frequency.

The corresponding output power is then given by

$$\text{SNR} = \frac{(3/2)(\text{CNR})B\beta^2 w_m^2 / w_b^3}{1 + (1/\text{CNR})(X^2/4 - 3X/8 + 1/2 - 1/4X)} \quad (2-16)$$

where  $X = B/w_b$ . The only assumptions made here were that  $w_b < B/2$  and that the signal and noise terms are additive.



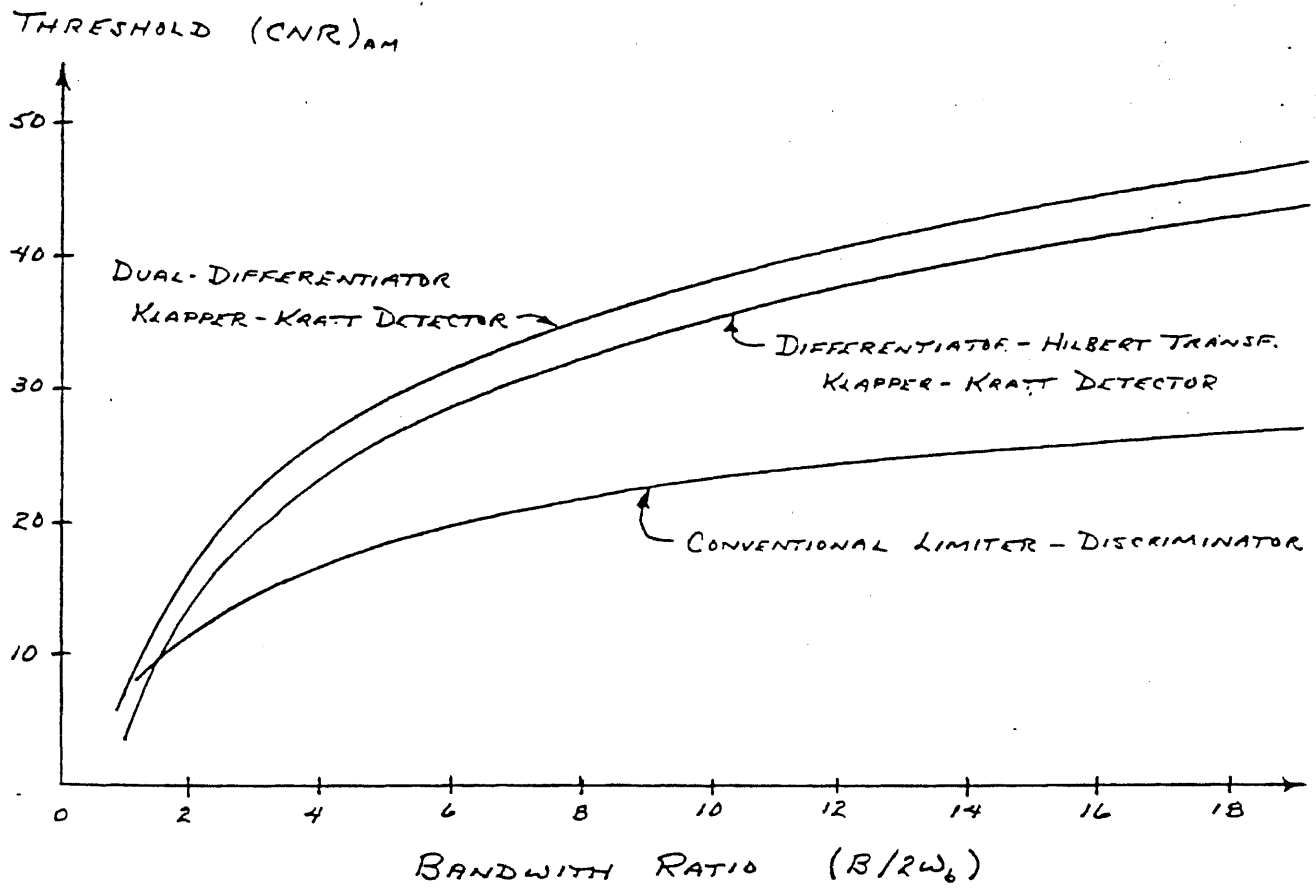


Figure 2-6. Threshold Characteristics

For a special case of high CNR, the denominator of Equation 2-16 becomes unity. And letting  $w_m = w_b$  for optimum performance, and using the relationship of (CNR) and  $(\text{CNR})_{\text{AM}}$ ,  $(\text{CNR}) = (\text{CNR})_{\text{AM}}(2w_b/B)$ , then the SNR for the high CNR conditions will be given by

$$\text{SNR}_{\text{high CNR}} = 3 \beta^2 (\text{CNR})_{\text{AM}} \quad (2-17)$$

which is identical to the expression for the region well above threshold of a limiter-discriminator(Ref. 4), i.e., the performance of the new detector, without using a limiter, is identical to a limiter-discriminator, well above the threshold region.

As indicated in Figure 2-5, the threshold point for an FM system is usually defined as the point where the SNR has dropped 1 dB more than that expected by the linear improvement region. Recalling Equation 2-16, this occurs where the denominator increases an amount above unity equivalent to 1 dB. The result may be given by

$$(\text{CNR}_{\text{AM}})_{\text{Th}} = 1.931(X^3/2 - 3X^2/8 + X/2 - 1/4) \quad (2-18)$$

In comparison, the SNR relationship for the detector of dual differentiator shown in Figure 1-4 is given by Tarbell(Ref.6) as

$$\text{SNR} = \frac{(3/2)(\text{CNR})B\beta^2 w_m^2 / w_b^3}{1 + (1/\text{CNR})(X^2/2 - 3X/4 + 1/2 - 1/8X)} \quad (2-19)$$

The corresponding equation for the threshold CNR is

$$(\text{CNR}_{\text{AM}})_{\text{Th}} = 1.931(X^3/2 - 3X^2/4 + X/2 + 1/8) \quad (2-20)$$

The results of Equation 2-17 and Equation 2-19 are shown in Figure 2-6 for various values of  $B/2w_b$ , along with the data for a conventional limiter-discriminator (Ref.5) for comparison. The new detector has a 3 dB improvement in threshold performance over the dual differentiator version shown in Figure 1-4. However, the new detector still has no improvement over the limiter-discriminator.

#### References - Chapter 2

1. E. Kratt, "Optimization of a New Linear FM Detector Using Digital Signal Processing Techniques," Chap. 3 A Doctoral Dissertation, NJIT, October 1982.
2. M. S. Corrington, "Frequency Modulation Caused by Common-and-Adjacent-Channel Interference," RCA Rev., Vol. 7, Dec. 1946.



3. P. F. Panter, Modulation, Noise, and Spectral Analysis, Chapter 14, McGraw Hill, 1965.
4. M. Schwartz, Information Transmission, Modulation, and Noise, Chapter 6, McGraw Hill, 1970.
5. J. Klapper and J. T. Frankle, Phase Locked and Frequency Feedback Systems, Chapter 7, Academic Press, 1972.
6. A. Tarbell and J. Klapper, "Noise performance of the Klapper-Kratt Low Delay FM Detector," NAT. TELECOM. CONF., Washington, D.C., Nov. 1979.

# CHAPTER III.

## IMPLEMENTATION

### 3.1 Introduction

A digitally implemented FM detector was designed by adapting the algorithms that will closely resemble the differentiator and Hilbert transformer of Figure 1-6 over the frequency band of interest. And the corresponding input samples were added and multiplied as required to perform the functions.

The differentiator and Hilbert transformer were realized using a finite impulse response (FIR), or non-recursive, digital filter design method. Such designs exhibit no phase errors, and have delays of approximately  $N/2$  times the sampling period, where  $N$  is the order of the network.

### 3.2 Network Order Evaluation

The coefficients for the FIR realizations of both differentiators and Hilbert transformers were derived using a computer program called EQFIR (Ref.1). The EQFIR program optimizes the results over a prescribed frequency range, which was selected as  $0.15 f_s$  to  $0.35 f_s$ , where  $f_s$  is the sampling frequency.<sup>1</sup>

These values will then generate a detector that is centered at half of the Nyquist frequency with relatively wide linear bandwidth of two-fifths of the Nyquist frequency, where the Nyquist frequency is a half of the sampling frequency.

The coefficients for selecting the network order  $N$  was computed and well evaluated by E. Kratt (Ref. 2) for differentiators with  $N = 5, 7,$  and  $9$  and for Hilbert transformers with  $N = 5, 7, 9,$  and  $11$ . The results are shown in Figures 3-1 and 3-2, respectively. The selection of the network order  $N$  was based on the minimum value that gave approximate results. A lower value of  $N$  also means a simpler algorithm for easier implementation and smaller values of delay. As a result,  $N = 7$  was chosen for both the differentiator and Hilbert transformer.

The coefficient of the differentiator and the Hilbert transformer were then computed for  $N = 7$  using EQFIR, and are shown in Table 3-1.

The equation for the frequency response of the detector was then derived, and is given by

$$E_o(F) = 1/2 \sum_{m=1}^N \sum_{n=1}^N (c_{dn} - c_{hn}) c_{hm} [\cos(m - n)2\pi F - \cos(N + 1 - n - m)2\pi F] \quad (3-1)$$

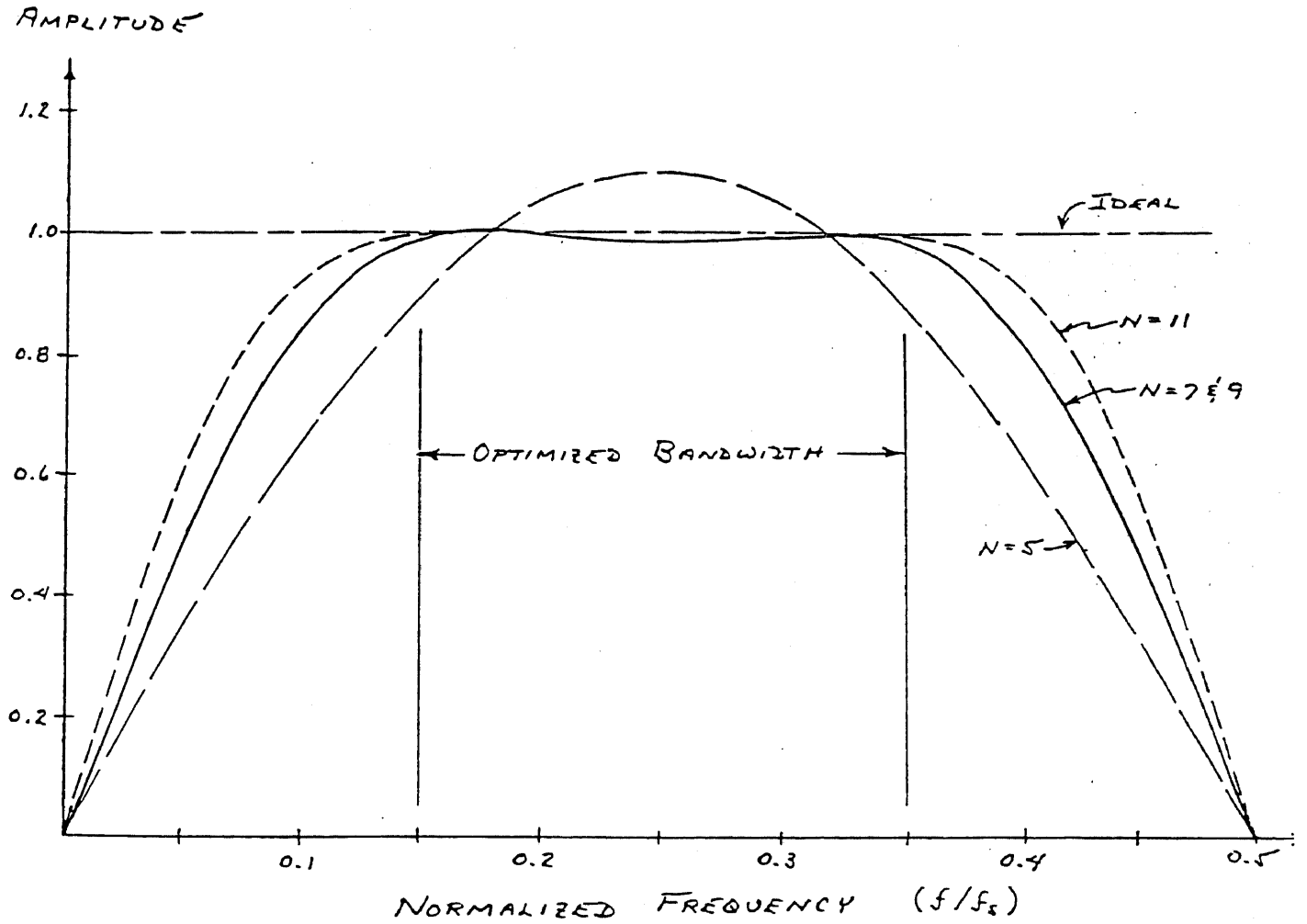


Figure 3-1. Frequency Response of Differentiators

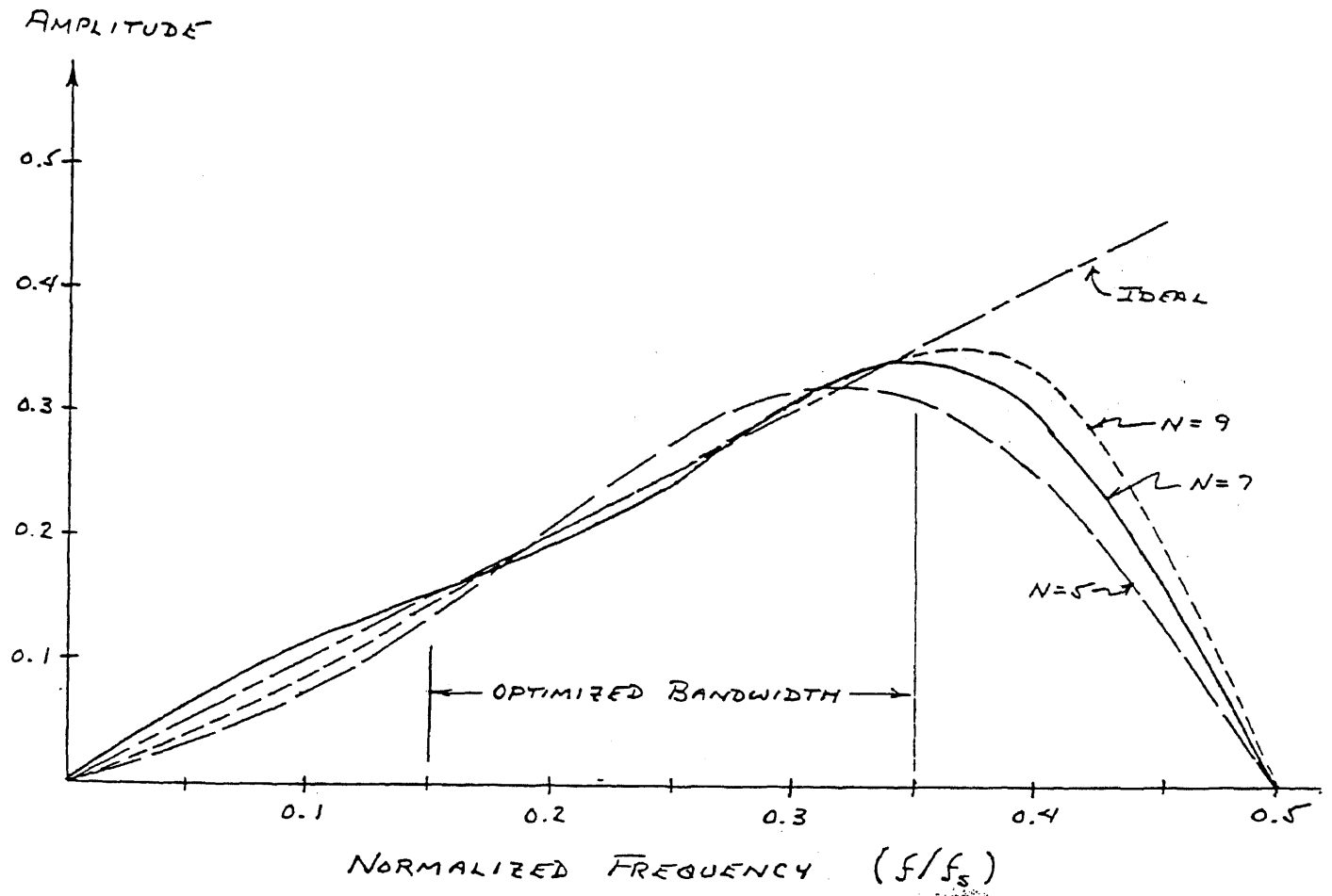


Figure 3-2. Frequency Response of Hilbert Transformers

TABLE 3-1  
Original Detector Coefficients  
(Impulse Response)

H (i)	Diff. Block	H. T. Block
H(1) = - H(7)	0.08223	0.08510
H(2) = - H(6)	- 0.19502	0.00240
H(3) = - H(5)	0.57944	0.58080
H(4)	0.00000	0.00000

where  $F$  is the normalized frequency to the sampling frequency,  $c_{dn}$  is  $n$ -th coefficient (or impulse response) of the differentiator and  $c_{hn}$  is the  $n$ -th coefficient of the Hilbert transformer.

The detector response was then computed using the coefficients for  $N = 7$  in Table 3-1 and Equation 3-1. The results are shown in Figure 3-3, which indicates that the response has a much greater linearity error than indicated by any of the individual components. This is because the particular errors of each block get multiplied when combined in the total detector, resulting in a much larger error.

### 3.3 Linearity Realization

Considerations were now given to optimizing the detector coefficients for linearity over the frequency range of interest. In order to retain certain necessary properties there had to be placed constraints on the coefficients.

First, the negative symmetry of the coefficients is required to achieve the linear-phase characteristic of the FIR block (actually a constant 90 degree phase). This requires that  $c_i = -c_{N+1-i}$ , and  $c_{(N+1)/2} = 0$ , since  $N$  is odd. The 90 degree phase shift properties of the components is required to maintain the quadrature relationships for carrier cancellation.

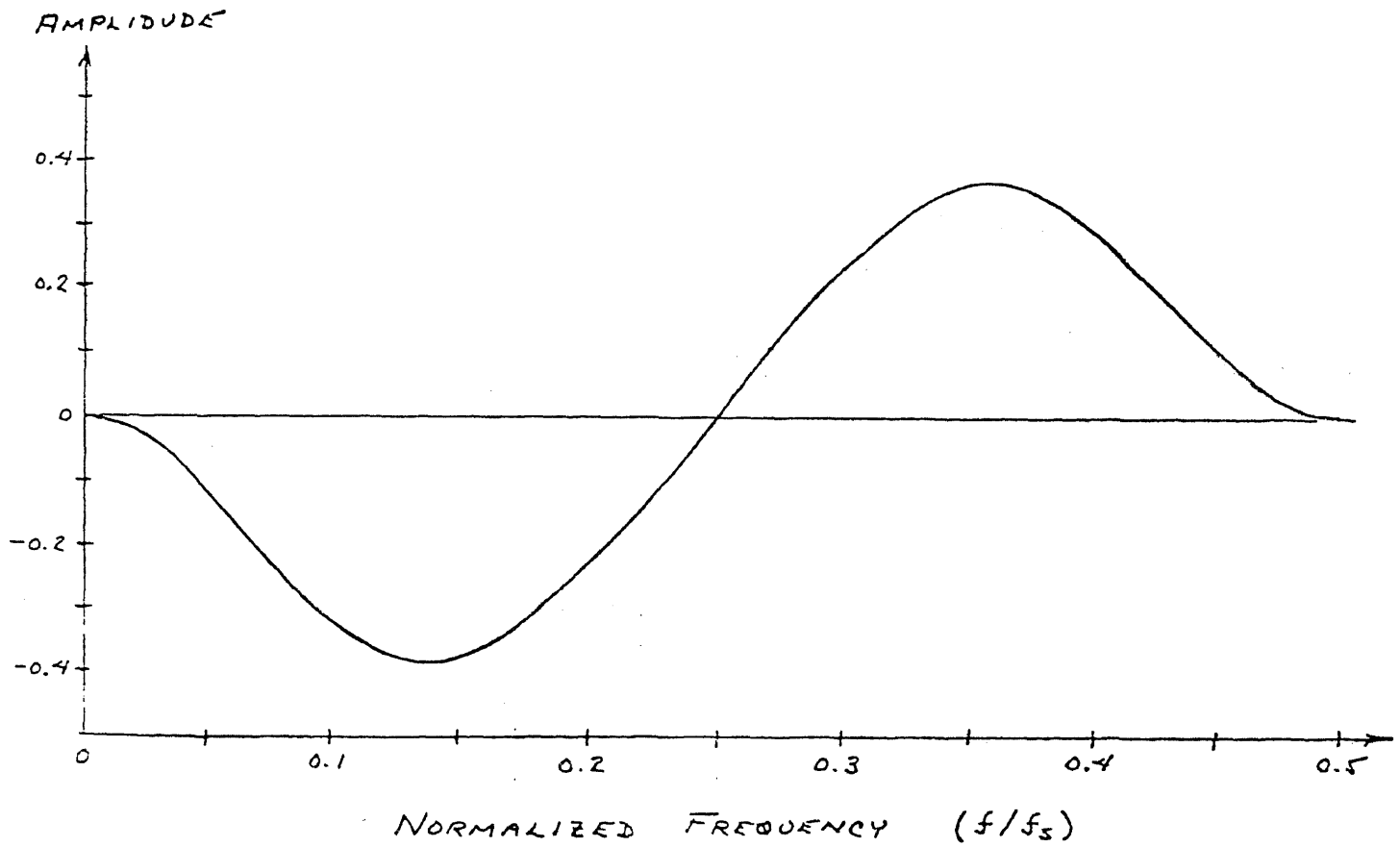


Figure 3-3. Detector Output

(Before Being Optimized)



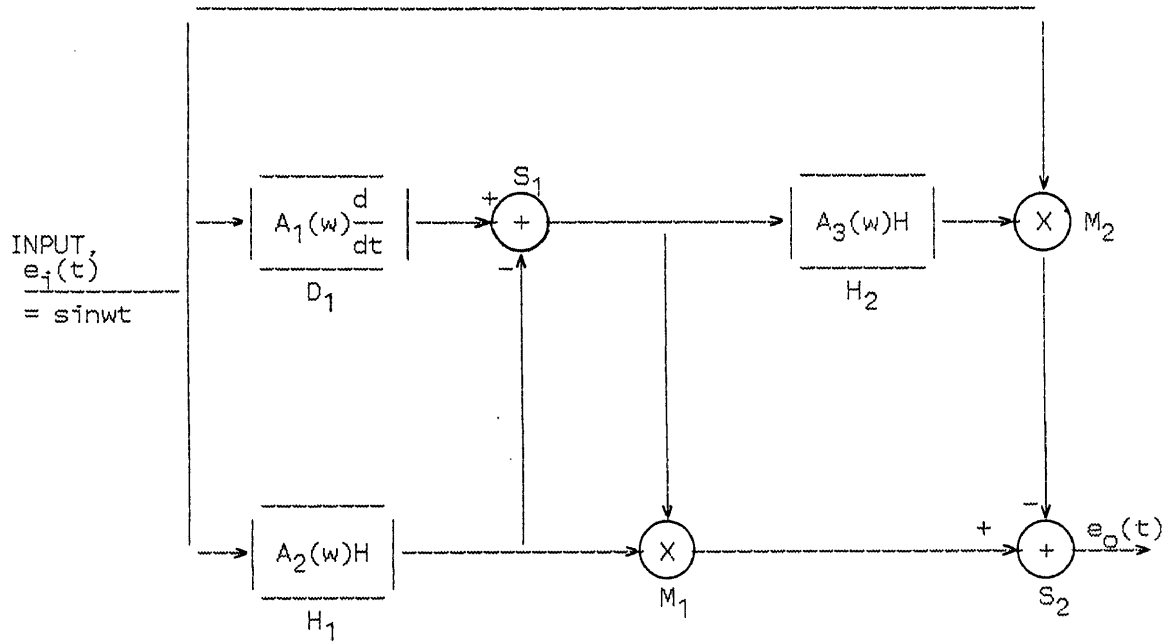


Figure 3-4. Non-Ideal Block Representation

As a result, only three values are required to define the seven general coefficients of each FIR block.

Next, the amplitude restraints are required. This may be determined by assuming that each FIR functional block is multiplied by a corresponding amplitude function of frequency  $F$ , as shown in Figure 3-4. These amplitude functions represent the non-ideal amplitude variations in the realization of each block.

Assuming an input  $e_1(t) = \sin 2\pi ft$ , the corresponding output is found to be given by

$$e_o(t) = [A_1(\omega) - A_2(\omega)] \cdot [A_2(\omega)\cos^2 \omega t + A_3(\omega)\sin^2 \omega t] \quad (3-2)$$

This equation shows that the carrier components will cancel exactly only if  $A_2(\omega) = A_3(\omega)$ . This means that the coefficients of the two Hilbert transformers should be identical. The linearity of the detector is then controlled by  $A_1(\omega)$  and  $A_2(\omega)$ , which may vary from unity and still give the desired result of  $e_o(t) = (w - 1)$  as long as they are related to the expression

$$A_1(\omega) = (1/\omega)[(\omega - 1)/A_2(\omega) + A_2(\omega)] \quad (3-3)$$

TABLE 3-2  
 Optimized Detector Coefficients  
 (Impulse Response)

H(1)	DIFF. BLOCK	H. T. BLOCK
H(1) = - H(7)	0.19019	0.19071
H(2) = - H(6)	- 0.21116	- 0.00157
H(3) = - H(5)	0.54117	0.54175
H(4)	0.00000	0.00000

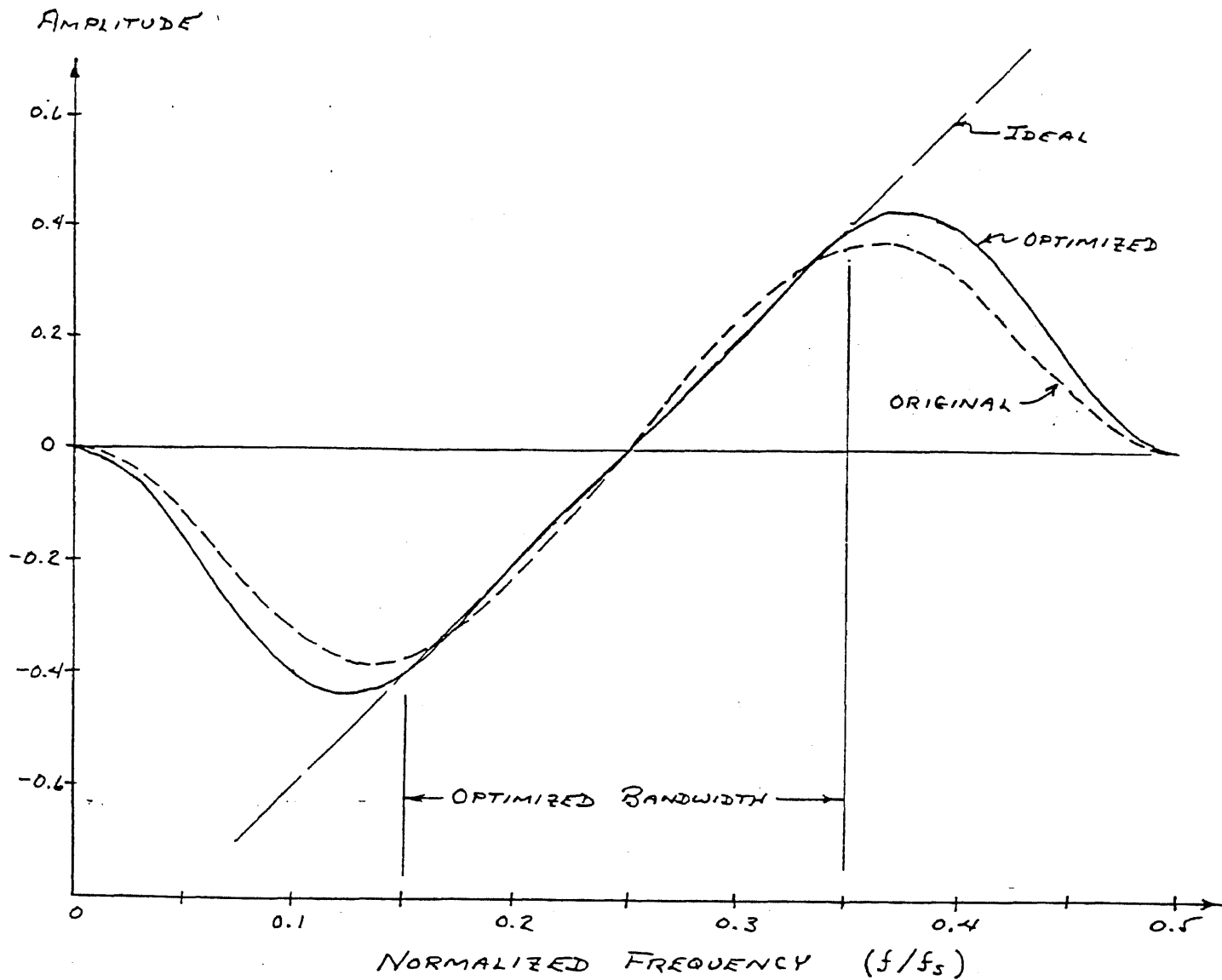


Figure 3-5. Detector Output with Linearity Optimization

And the optimized coefficients were obtained by computer routines which were generated to minimize a least squares linearity error function using the Fletcher-Powell algorithm (Ref. 3), and are shown in Table 3-2. The corresponding optimized detector output is shown in Figure 3-5, where it is compared with both the original detector output and the ideal output. The output is found to be extremely linear over the optimized frequency range, and with substantial improvement over the original response.

#### 3.4 Algorithm Simplification

Observing the coefficients given in Table 3-2, the coefficients for the differentiator and Hilbert transformer blocks are found to be practically identical for both the first and third values. Referring back to Figure 1-6, the outputs of D1 and H1 are subtracted in summer S1. Since multiplying an input sample by two different coefficients and then taking the difference of the results is equivalent to multiplying the input sample by the difference of the two coefficients, then the functions of D1, H1 and S1 may be replaced by a single block, as shown in Figure 3-6, with the coefficients equal to  $c_{d1} - c_{h1}$ . Therefore the first and third coefficients would be zero, while the second coefficient be -0.20959.

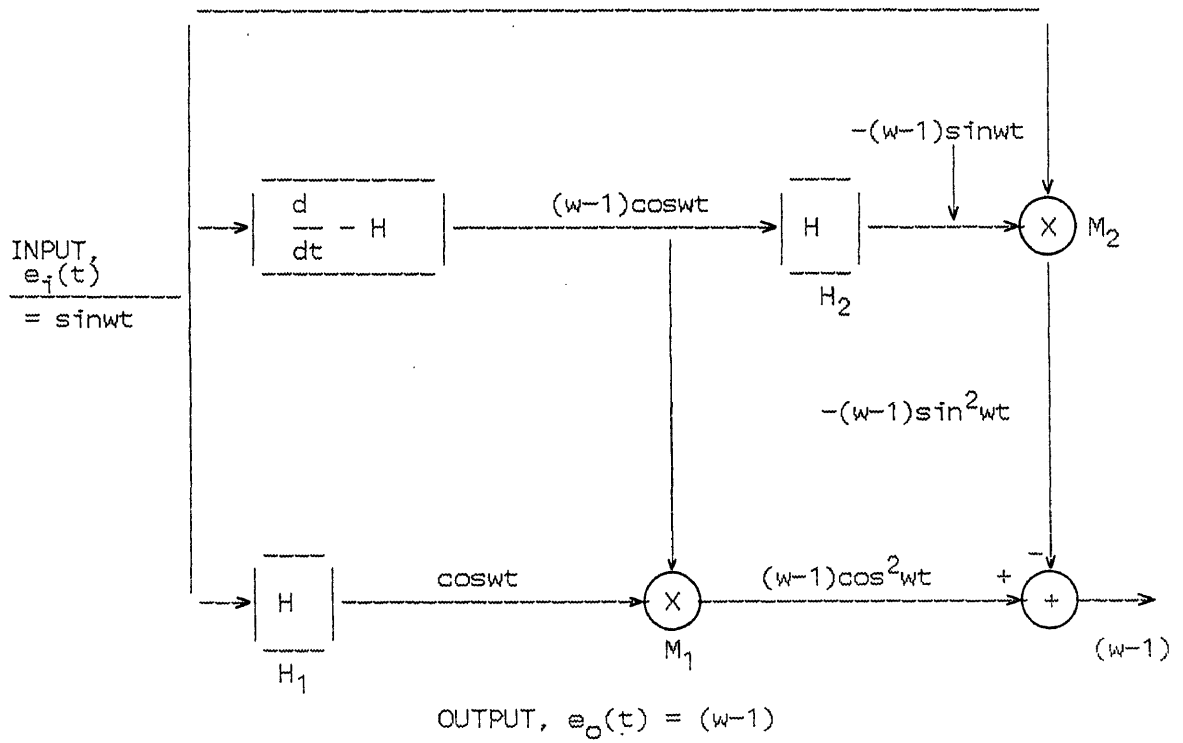


Figure 3-6. Simplified Detector Block Diagram

The fact that two of the coefficients of this new block are zero needs to be observed. Recall that the output of S1 is actually the output of the discriminator before synchronous detection. The frequency response should therefore be zero at the center frequency ( $F = 0.25$ ), and have odd symmetry around this point. A negative value, in this case, means a phase reversal. Comparing this with the theoretical frequency response of a FIR block (Ref. 2), which is given as

$$H(F) = j \sum_{n=1}^{(N-1)/2} 2c_n \sin(N + 1 - 2n)\pi F \quad (3-4)$$

only the term for  $n = 2$  produces odd symmetry about  $F = 0.25$ . The other two terms have even symmetry, and should therefore be zero. By observing Equation 3-4 for larger values of  $N$ , alternate terms will be seen to have even symmetry and therefore must be equal to zero. As a result, similar simplifications may also be made for higher order detectors of different bandwidths, as long as  $F_0 = 0.25$ .

Since the D-H block has only one non-zero coefficient, then only one subtraction and one multiplication is needed to realize the functional block. The Hilbert transformers, however, require three times as much.

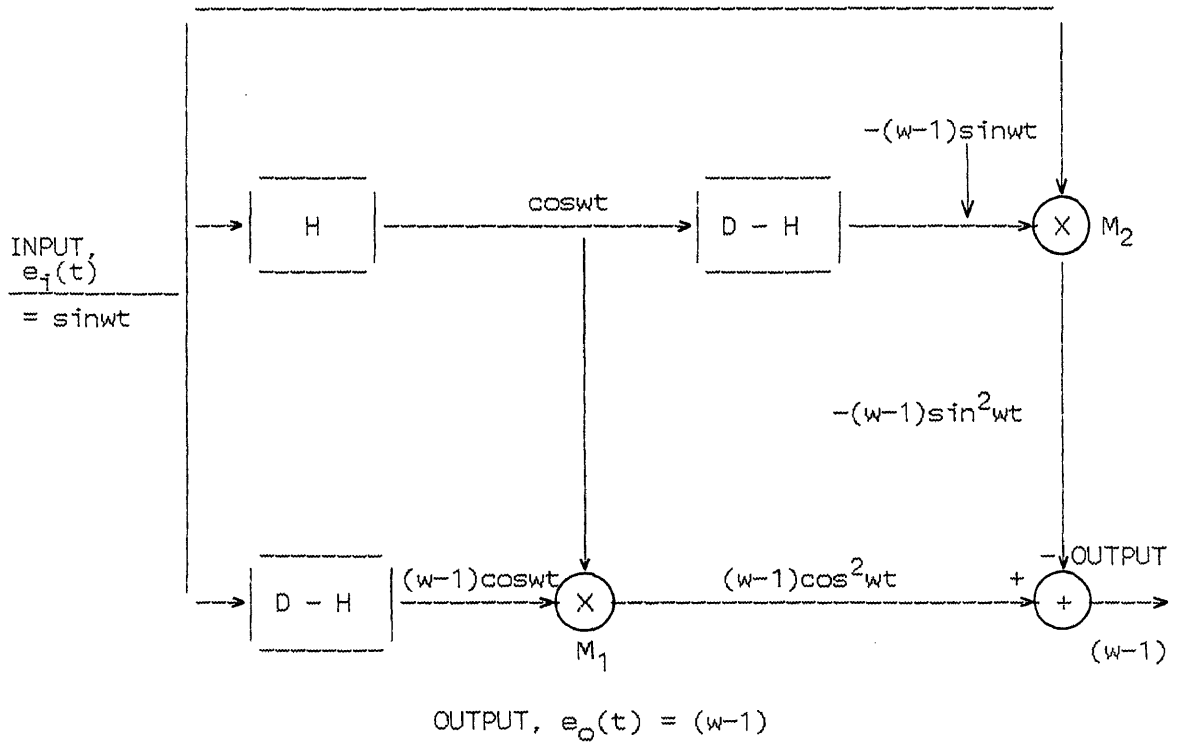


Figure 3-7. Block Diagram of the Equivalent Simplified Detector



So, we would like to reduce the number of Hilbert transformers, which would also reduce the computation time. The dual of the detector of Figure 3-6, which resulted in the configuration shown in Figure 3-7, was taken to accomplish this objective. The two detectors are equivalent in performance since the multiplier inputs are still identical.

### 3.6 Software Description

A FIR realization diagram is shown in Figure 3-8, which is based on the algorithm for the optimized detector in Figure 3-7. Two arrays of data should be arranged in the memory. One array holds ten consecutive input sample voltages, while the other contains seven consecutive outputs of the Hilbert transformer. The previous samples appear to the right side.

Following the diagram, where the subscripts of E and H denote the number of delays, the value of  $H_3$  which is the output of the Hilbert transformer is generated using

$$H_3 = (E_0 - E_6)c_{H1} + (E_2 - E_4)c_{H3} \quad (3-5)$$

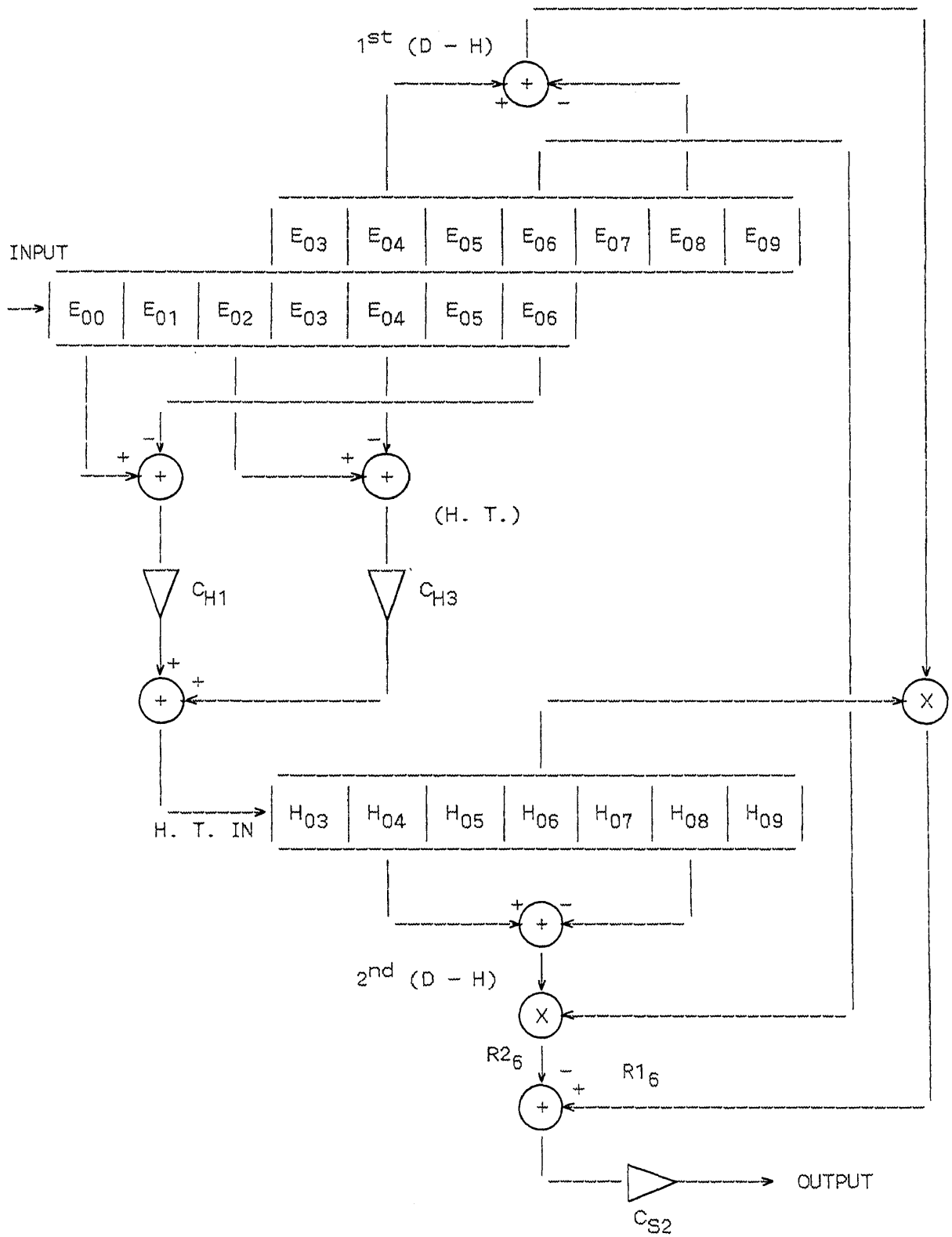


Figure 3-8. Diagram of the Implementation Algorithm

which is possible to be calculated by two subtractions and two multiplications ( Equation 3-5 ) instead of four multiplications and two subtractions of the original algorithm in Figure 3-7 due to the symmetry of the coefficients.

The output of the second D-H block, called R2, is obtained from

$$R2_6 = (H_4 - H_8)c_{S2} \quad (3-6)$$

The delays are three sample periods for each block realization, or six for the total detector, and that may be seen by observing the subscripts. In a similar way, the output of the first D-H block is given by

$$R1_6 = (E_4 - E_8)c_{S2} \quad (3-7)$$

and finally, the output of the detector is found using

$$\text{OUTPUT} = R1_6 H_6 - R2_6 E_6 \quad (3-8)$$

Then the final result is ready to be outed to an output port. Then the values in the arrays are shifted to the right by one, with a new sample entering at the left, and the whole procedure is repeated.

Observe in the above Equations, that only three different values of coefficients are required to perform the algorithm. The values of these coefficients are  $c_{H1} = 0.19045$ ,  $c_{H2} = 0.54146$  and  $c_{S2} = -0.20959$ .

### 3.5 System Configuration

To implement analog signals by digital means, there are at least A/D and D/A circuits incorporating LPFs for anti-aliasing and post detection recovering, and a digital signal processor(DSP). The digital signal processor may be substituted by a general purpose digital micro-processor, but in this case, the processing speed will be reduced in comparison with the special purpose DSP (Ref. 4). Considering these conditions of the speed and ease of implementation, the INTEL 2920 DSP was chosen to realize the algorithm of Figure 3-8. The INTEL 2920 DSP(Ref. 5), whose block diagram is given in Figure 3-9, is comprised of a digital micro-processor, a 9-bit A/D converter, 24-bit program-store EPROMs, 24-bit scratch-pad data RAMs, a D/A converter, and a Sample and Hold circuit with I/O ports. The architecture and instruction sets were developed to perform precise and high speed signal processing.

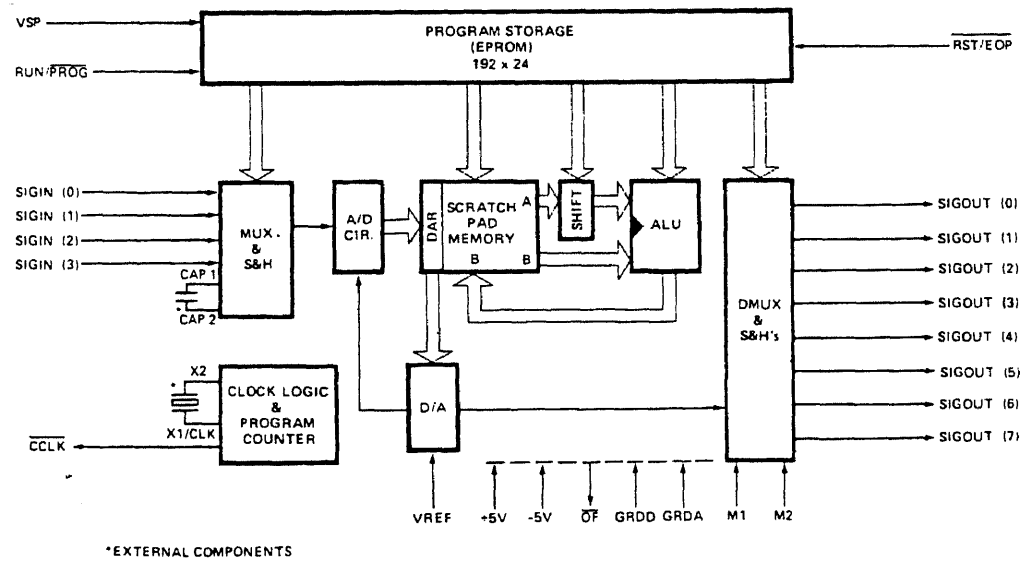


Figure 3-9. 2920 Block Diagram

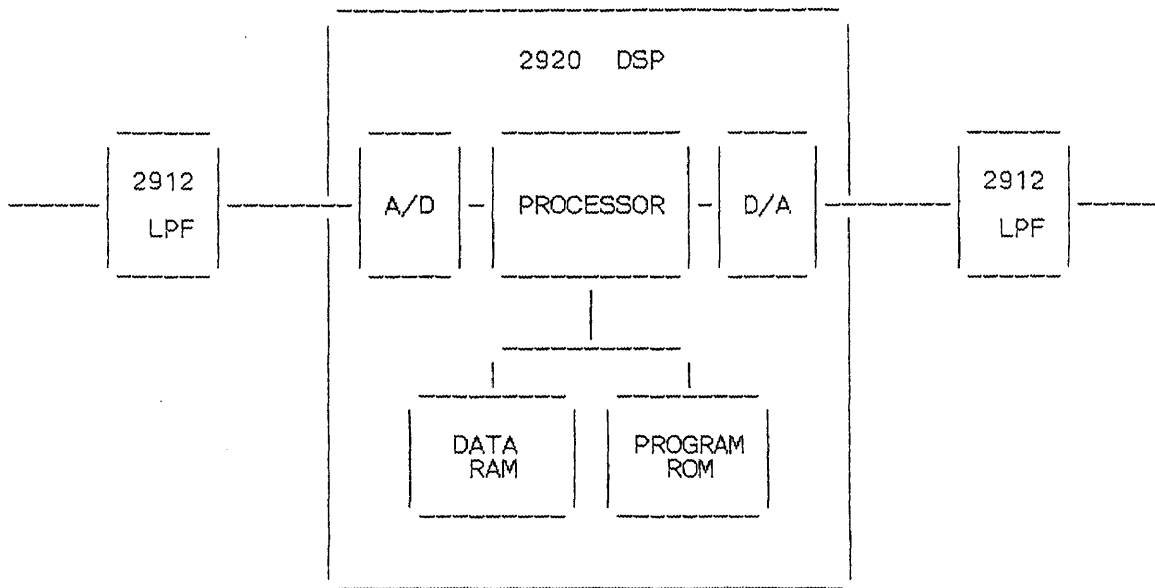
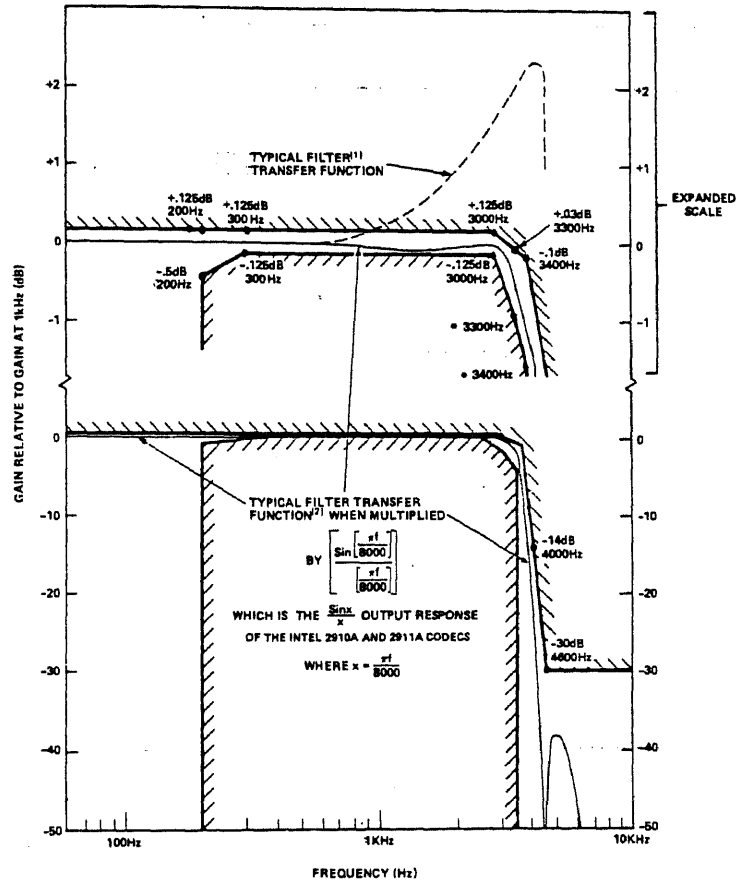


Figure 3-10. A Block Diagram of the System Configuration



NOTES:  
 1. TYPICAL TRANSFER FUNCTION OF THE RECEIVE FILTER AS A SEPARATE COMPONENT.  
 2. TYPICAL TRANSFER FUNCTION OF THE RECEIVE FILTER DRIVEN BY THE SAMPLE AND HOLD OUTPUT OF THE INTEL 2910A AND 2911A CODECS. THE COMBINED FILTER/CODEC RESPONSE MEETS THE STATED SPECIFICATIONS.

	2912	2912-3
FREQ	2912-4	2912-5
3300Hz	D3/D4	CCITT
3400Hz	-1.4	-70

Figure 3-11. The LPF Characteristics of 2912

The basic system configuration of the detector is shown in Figure 3-10 which is comprised of two LPFs and one INTEL-2920 DSP. As shown in Figure 3-10, two INTEL-2912 chips were used as a pre-sampling LPF for anti-aliasing and a post detection LPF for removing high-order multiples. The characteristic of the LPF is shown in Figure 3-11. From the basic system configuration, we may observe that all the digital signals are processed within the 2920 DSP. The 2920 DSP has 4 analog input ports and 8 output ports which can be used as analog and/or digital. For the system configuration the input port No. 0 and output port No. 0 are used. Inside of the 2920, input and output analog signals are accomplished by sample and hold circuits, and sampled data to and from the processor is accomplished through DAR using the 9-bit A/D and D/A converter, where one of the bits is used for the polarity.

### 3.7 Realization

The detector of Figure 3-10 was realized using a SDK-2920 system development kit, which is used as a convenient laboratory tool for the experiments, and is comprised of two parts, one for system development and another for system experiment.



The processing speed and the sampling period is determined by the number of instructions in the program and clock cycle of the processor. The processor executes its programs at typically 6,500 times a second when used with a 5 MHz clock and full program memory (i.e., 192 steps of program).

Using the configuration shown in Figure 3-8, which requires five multiplications, one addition, and five subtractions, the realization of the detector needed about 100 steps of program which could execute sampling rates of 12,500 times a second. For the ease of using the carrier frequency, the sampling period was selected as 10,000 times a second, which require 125 steps of program. However, the characteristics of the 2920 DSP requires executing 4 instructions together, therefore, 124 steps were chosen to implement the detector. These results were incorporated into the program named FMDET2920.KRT, which was used to perform the algorithm in a real time realization, and are given in Figure 3-12. The program begins with handling input samples followed by algorithm computations. The latter portion of the program shifts the data arrays in preparation for the next loop.

Since the FMDET2920.KRT uses 124 steps of instructions and the processor uses the 5 MHz clock, the

resulting sample periods will be approximately 10,000 samples a second and then the detector operating range will be 1,500 to 3,500 Hz and its center frequency be 2,500 Hz.

### References - Chapter 3

1. J. H. McClellan, T. W. Parks and L. R. Rabiner, "FIR Linear Phase Filter Design Program," Programs for Digital Signal Processing, Chapter 5-1, IEEE Press, New York, 1979.
2. E. Kratt, "Optimization of a New Linear FM Detector Using Digital Signal Processing Techniques," A Doctoral Dissertation, NJIT, October 1982.
3. R. Fletcher and M. J. D. Powell, "A rapidly convergent descent method for minimization," Computer J., Vol. 6, No. 2, July 1963.
4. W. D. Stanley, G. R. Dougherty and R. Dougherty, "Digital Signal Processing," Chapter 15. Reston Publishing Company, Inc. Reston, Virginia, 1984.
5. INTEL, "The 2920 Analog Signal Processor Design Handbook," Intel Corporation, August 1980.

FMDET2920.KRT

<u>STEP</u>	<u>INST</u>	<u>DST</u>	<u>SRC</u>	<u>SHFT</u>	<u>ANLG</u>	
0	SUB	DAR	DAR	R00	NOP	CLEAR DAR FOR NEW INPUT
1					IN0	INPUT 6 TIMES CONSECUTIVELY
2					IN0	
3					IN0	
4					IN0	
5					IN0	
6					IN0	
7					NOP	2 NOP'S FOR TIME CONST.
8					NOP	
9					CVTS	CONVERT SIGN BIT
10	ADD	DAR	KM2	R00	CND6	A/D CONVERSION INSTRUCTION
11					NOP	
12					NOP	
13					CVT7	
14					NOP	
15					NOP	
16					CVT6	
17					NOP	
18					NOP	
19					CVT5	
20					NOP	
21					NOP	
22					CVT4	
23					NOP	
24					NOP	
25					CVT3	
26	LDA	Y00	Y00	R00	CND4	
27					NOP	
28					CVT2	
29	LDA	Y00	Y00	R00	CND4	
30					NOP	
31					CVT1	
32	LDA	Y00	Y00	R00	CND4	
33					NOP	
34					CVT0	
35					NOP	
36					NOP	
37	LDA	E00	DAR	R00	NOP	STORE SAMPLE AT DATA ARRAY
38	LDA	Y00	E00	R00	NOP	BEGIN FIRST BLOCK CALCULATION
39	SUB	Y00	E06	R00	NOP	
40	LDA	A00	Y00	R03	NOP	MULTI CH1=14141(0.19045)

Figure 3-12. Real-time Execution Program

41	ADD	A00	Y00	R04	NOP	MULTIPLICATION CONTINUES
42	ADD	A00	Y00	R09	NOP	
43	ADD	A00	Y00	R10	NOP	
44	LDA	Y00	Y00	R10	NOP	
45	ADD	A00	Y00	R05	NOP	A00 CONTAINS CALCUL RESULT
46	LDA	Y00	E02	R00	NOP	SECOND BLOCK BEGIN
47	SUB	Y00	E04	R00	NOP	
48	LDA	B00	Y00	R01	NOP	MULTI CH3=42517(0.54146)
49	ADD	B00	Y00	R05	NOP	
50	ADD	B00	Y00	R07	NOP	
51	ADD	B00	Y00	R09	NOP	
52	ADD	B00	Y00	R11	NOP	
53	LDA	Y00	Y00	R10	NOP	
54	SUB	B00	Y00	R05	NOP	
55	ADD	B00	A00	R00	NOP	ADDS 1ST & 2ND RESULTS
56	LDA	F03	B00	R00	NOP	STORE RESULT AT HILBERT TRANS
57	LDA	Y00	E04	R00	NOP	3RD BLK BEGIN
58	SUB	Y00	E08	R00	NOP	
59	ABS	C00	F06	R00	NOP	TAKE ABSOLUTE VALUE OF F06
60	LDA	DAR	C00	R00	NOP	LOAD DAR WITH ABS VAL OF F06
61	XOR	C00	C00	R00	NOP	CLEAR C00 FOR NEW DATA
62	LDA	C00	Y00	R01	CND7	MULTI D-H & H.T. OF F06
63	ADD	C00	Y00	R02	CND6	
64	ADD	C00	Y00	R03	CND5	
65	ADD	C00	Y00	R04	CND4	
66	ADD	C00	Y00	R05	CND3	
67	ADD	C00	Y00	R06	CND2	
68	ADD	C00	Y00	R07	CND1	
69	ADD	C00	Y00	R08	CND0	
70	LDA	C01	C00	R00	NOP	
71	SUB	C01	C01	L01	NOP	
72	LDA	DAR	F06	R00	NOP	
73	LDA	C00	C01	R00	CNDS	TREAT SIGN OF THE MULTI
74	LDA	Y00	F04	R00	NOP	4TH BLK BEGIN
75	SUB	Y00	F08	R00	NOP	
76	ABS	D00	E06	R00	NOP	TAKES ABSOLUTE VAL OF E06
77	LDA	DAR	D00	R00	NOP	
78	XOR	D00	D00	R00	NOP	CLEAR D00 FOR NEW CALCUL
79	LDA	D00	Y00	R01	CND7	MULTI 2ND D-H & INPUT(E06)
80	ADD	D00	Y00	R02	CND6	
81	ADD	D00	Y00	R03	CND5	
82	ADD	D00	Y00	R04	CND4	
83	ADD	D00	Y00	R05	CND3	
84	ADD	D00	Y00	R06	CND2	
85	ADD	D00	Y00	R07	CND1	

Figure 3-12 (continued)

86	ADD	D00	Y00	R08	CND0	
87	LDA	D01	D00	R00	NOP	TREAT SIGN
88	SUB	D01	D01	L01	NOP	
89	LDA	DAR	E06	R00	NOP	
90	LDA	D00	D01	R00	CNDS	D00 HAS RESULT OF 4TH BLK
91	SUB	C00	D00	R00	NOP	5TH BLK BEGIN
92	XOR	D00	D00	R00	NOP	CLEAR D00 FOR NEW DATA
93	SUB	D00	C00	R03	NOP	
94	SUB	D00	C00	R04	NOP	
95	SUB	D00	C00	R06	NOP	
96	SUB	D00	C00	R08	NOP	
97	SUB	D00	C00	R09	NOP	
98	SUB	D00	C00	R11	NOP	
99	SUB	D00	C00	R13	NOP	
100	LDA	DAR	D00	R00	NOP	DAR CONTAINS RESULT TO BE OUT
101	LDA	E08	E07	R00	NOP	SHIFT SAMPLES
102	LDA	E07	E06	R00	NOP	
103	LDA	E06	E05	R00	NOP	
104	LDA	E05	E04	R00	NOP	
105	LDA	E04	E03	R00	NOP	
106	LDA	E03	E02	R00	NOP	
107	LDA	E02	E01	R00	NOP	
108	LDA	E01	E00	R00	NOP	
109	LDA	F08	F07	R00	NOP	
110	LDA	F07	F06	R00	NOP	
111	LDA	F06	F05	R00	NOP	
112	LDA	F05	F04	R00	NOP	
113	LDA	F04	F03	R00	NOP	
114					CND2	
115					OUT2	PORT 2 IS DUMMY PORT
116					OUT2	
117					OUT0	OUTPUT TO PORT 0 TWO TIMES
118					OUT0	
119					NOP	PSEUDO-INST FOR TIMING
120					EOP	END OF PROGRAM
121					NOP	
122					NOP	
123					NOP	RETURN TO 0; LOOP FINISH

Figure 3-12 (continued)

CHAPTER IV .  
DETECTOR PERFORMANCE

4.1 Introduction

The actual response of the detector was measured under steady-state conditions, the result of which are shown in Figure 4-1. Compared with the theoretical response shown in Figure 3-5( which is optimized ), the two curves were found to be almost identical.

As predicted by the fold-over property of sampled systems, the detector output was found to have a mirror image( shown in Figure 4-2 ) for the frequencies immediately above the Nyquist frequency( i.e., 5,000 to 10,000 Hz ), where the Nyquist frequency is half of the sampling frequency(Ref. 1). From the sampling frequency of 10,000 Hz and its multiples, the detector response is repeating its baseband outputs, while an inverted baseband response occurs just below each of these frequencies.

Recalling that the sampling frequency is based on the modulation frequency bandwidth and not the carrier, a frequency translation may also be incorporated into the detector, as shown in Figure 4-2, as long as the input sampling circuits give a reasonable response.

The actual performance of the detector was observed using modulated input waves under both narrow and wide-band conditions. Also an evaluation of the detector under sinusoidal and noise interference conditions was done.

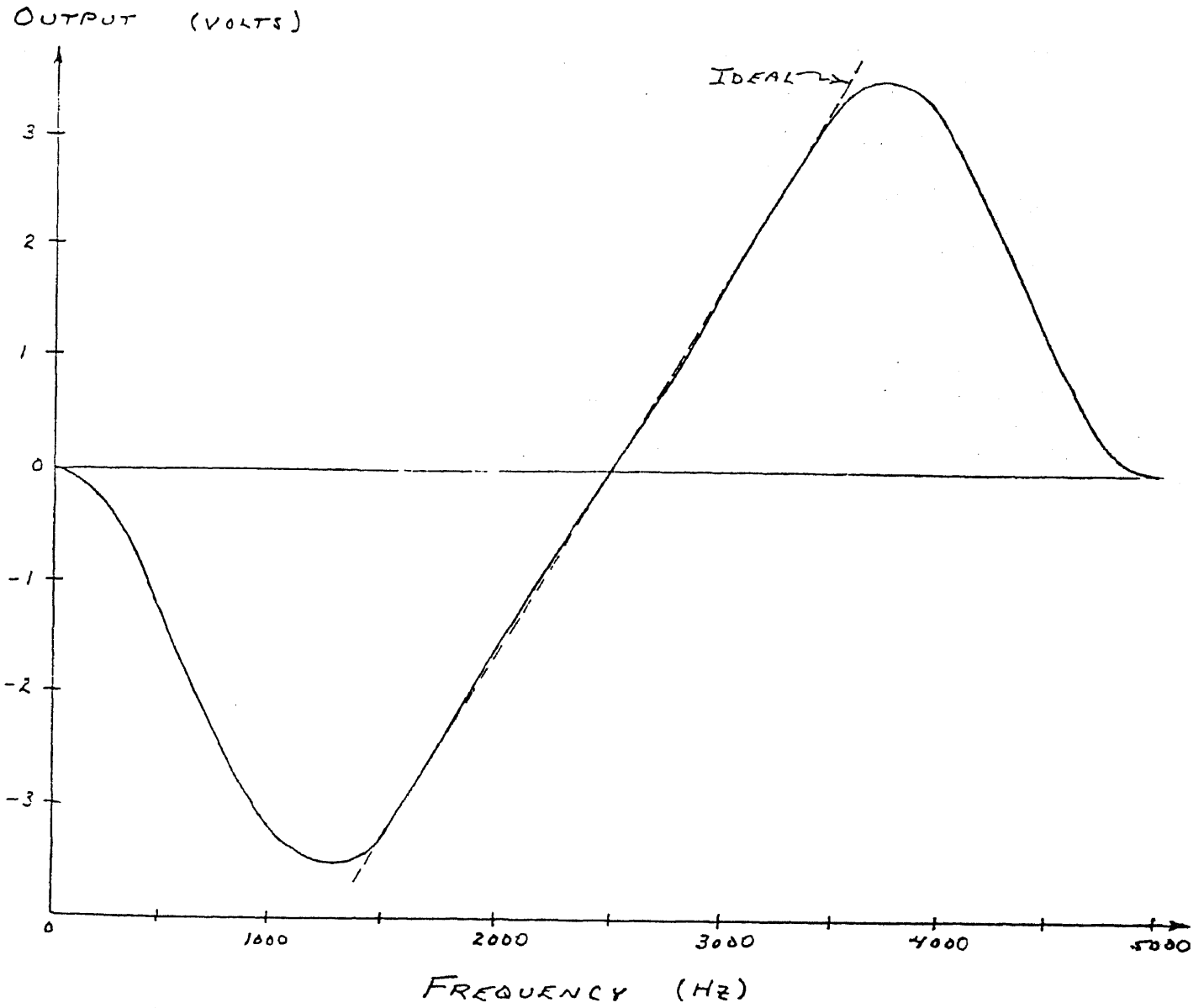
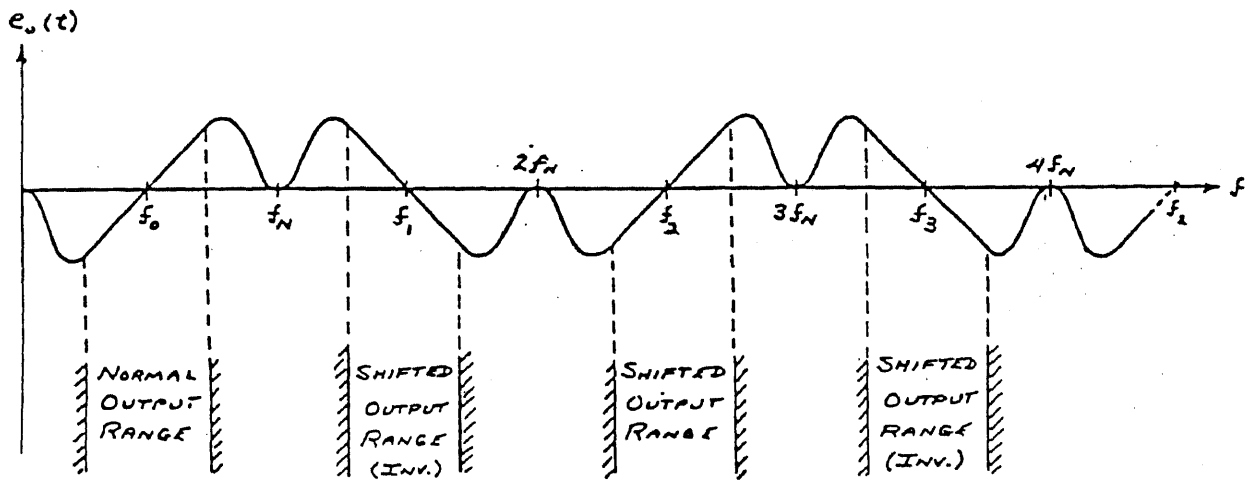


Figure 4-1. Actual Response of the detector



NOTE:

1.  $f_N = \text{NYQUIST FREQUENCY}$
2.  $f_s = 2f_N = \text{SAMPLING FREQUENCY}$

Figure 4-2. The Fold-over Property of the Detector



#### 4.2 Narrow-Band Performance

An FM modulated signal source was derived from a voltage controlled oscillator ( VCO ), which was modulated by a waveform generator. Adjusting the modulation index by controlling the output voltage and modulation frequency of the waveform generator, the input signal was narrow-band FM. The modulation frequency was selected as 1000 Hz

Figure 4-3 represents the waveform of the detector input terminal. The output waveforms of the detector for the narrow-band response is shown in Figure 4-4, where the upper curves represent the modulation signal while the lower curves represent the output of the detector prior to the LPF.

#### 4.3 Wide-Band Performance

In order to test the wide-band performance of the new detector, the modulation index was increased but with the proviso that the modulated signal band-width remains within the detector's operating range. If the modulation index increased too much, the detector output is no longer linear with the input modulation signal due to the fold-over characteristics of the detector. The modulation signal frequency for the test was 100 Hz (that may have 10 side-bands within its operating range) for all waveforms of sine-wave, triangular-wave and square-wave.

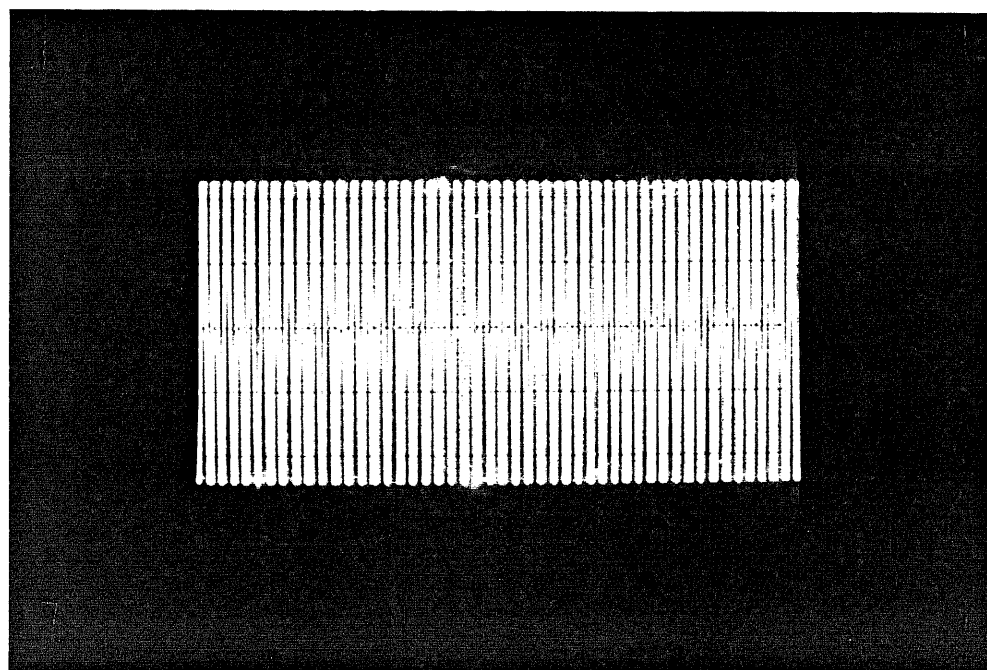
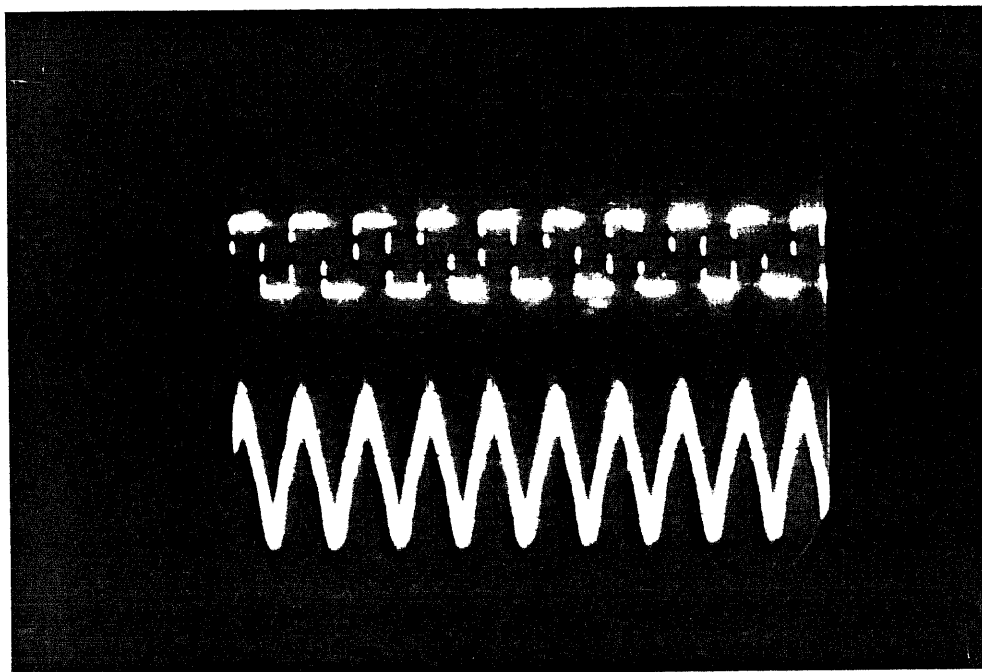
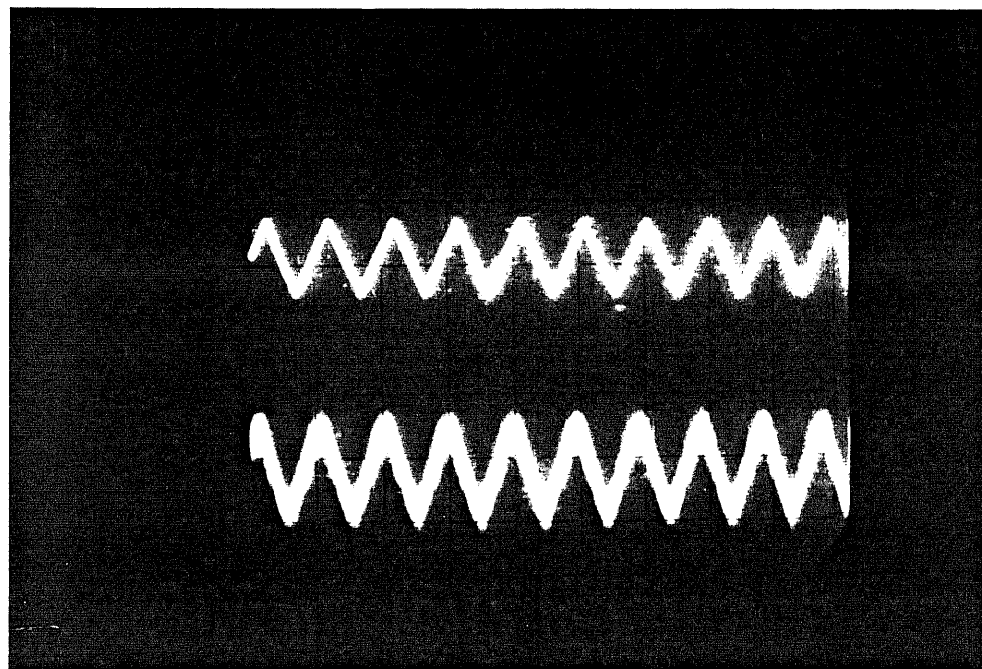


Figure 4-3. Detector Input Wave-Form

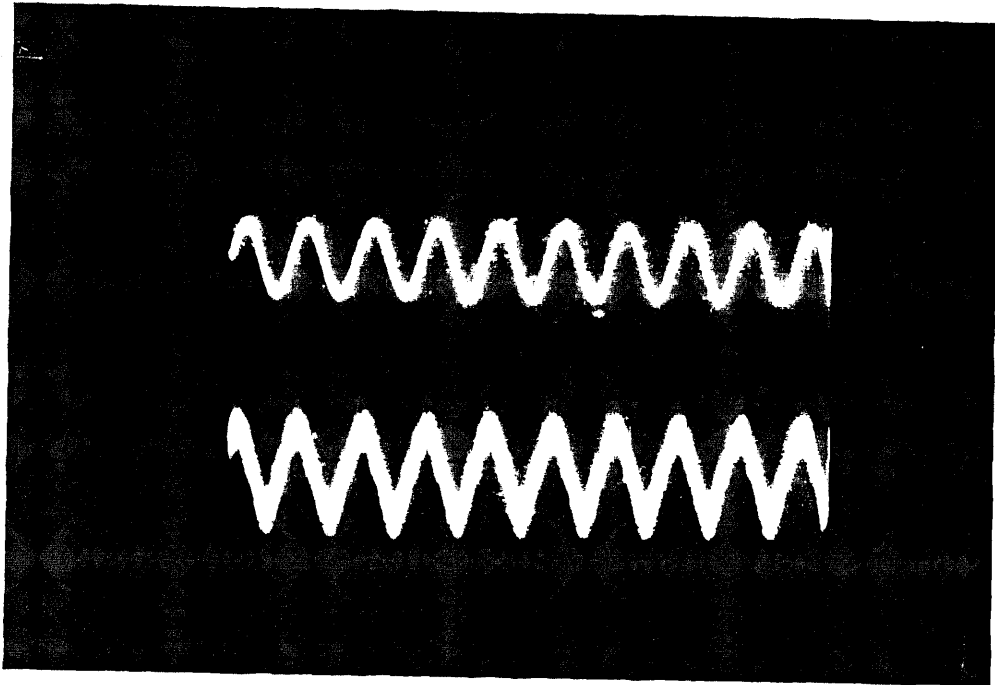


a) Detector Output for Rectangular-Wave



b) Detector Output for Triangular-Wave

Figure 4-4. The Detector Response for Narrow-Band



c) Detector Output for Sine-Wave

- The output waveforms for the above three cases are almost identical, which means that the FM signal bandwidth is limited and then have no harmonics for the modulation signal except the fundamental frequency.

Figure 4-4. Detector Response for Narrow-Band FM

(Continued)

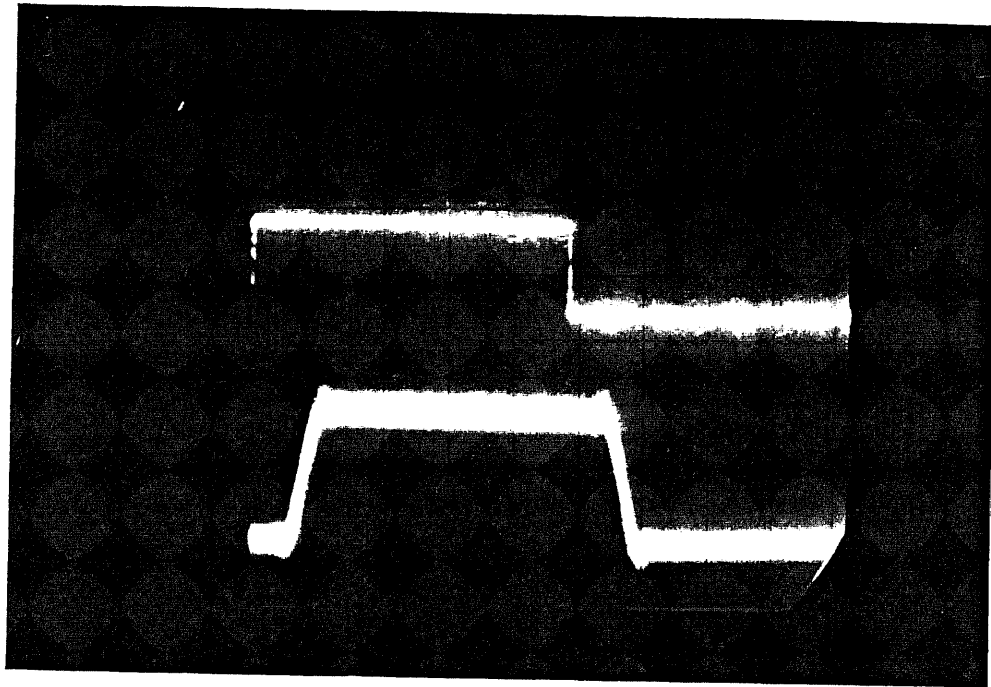
The performance is essentially identical to that of the narrow-band case.

By comparing the phases of the two waveforms shown in Figure 4-5, one from modulation signal another from detector output, the system delay was measured, and that a total delay of approximately 0.7 ms was observed.

This delays occur mainly from the FIR implementation by 6 delays of the sampling period and from the Program Realization by about one delay( which may be observed from Figure 3-12 where the execution time difference between an input and an output is almost one period). Figure 4-5 shows system delay and Figure 4-6 shows wide-band detector responses for the various modulation wave-forms.

#### References - Chapter 4.

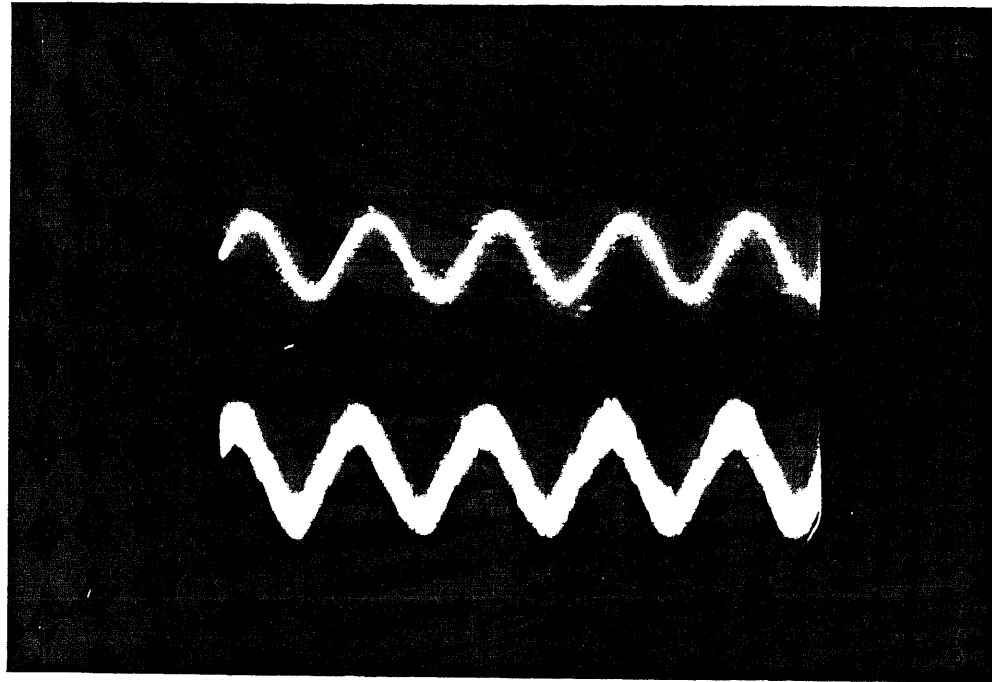
1. S. Stearns, Digital Signal Analysis, Hayden, 1975.



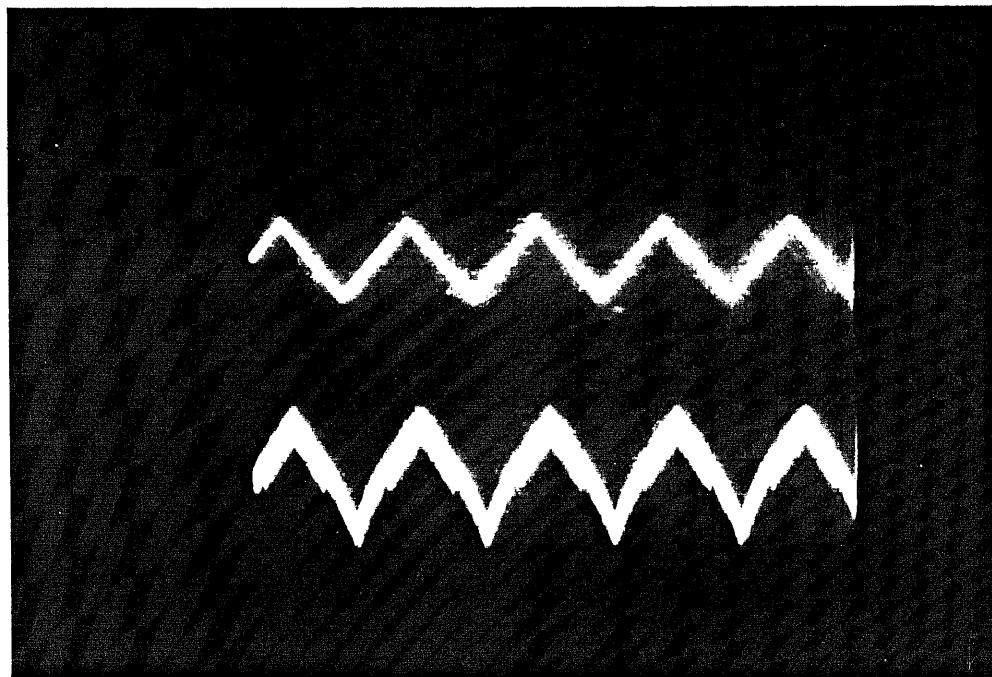
- The scale of the oscilloscope is 1 msec/div.

- The picture shows that about 0.7 msec of system delay and 0.3 msec of rising time

Figure 4-5. Detector Response for System Delay

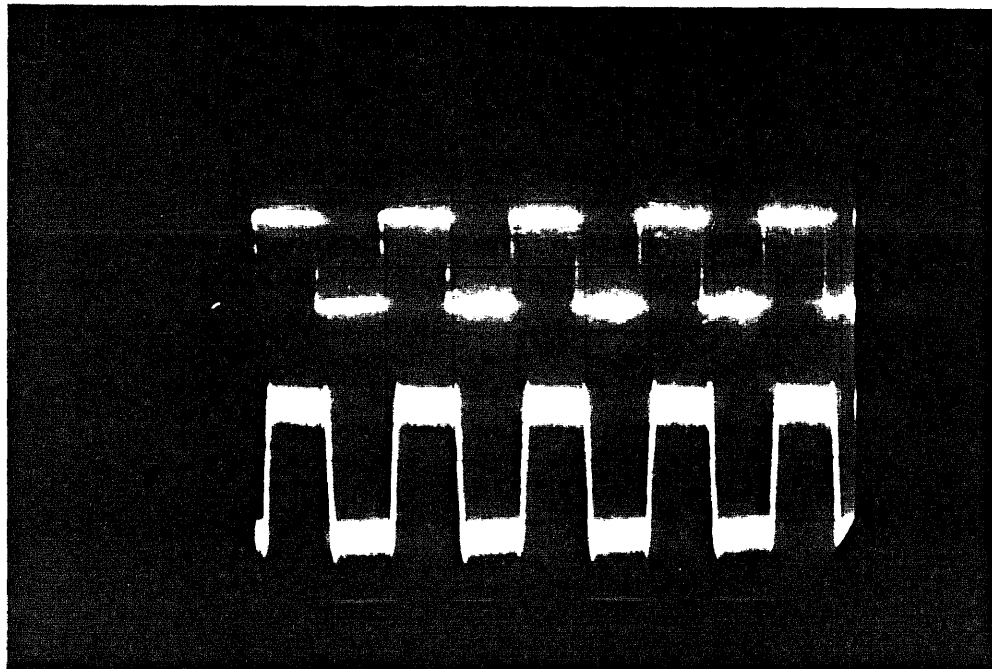


a) Sine-Wave Response



b) Triangular-Wave response

figure 4-6. Detector Responses of Wide-Band FM



c) Rectangular-Wave Response

Figure 4-6. Detector Response of Wide-Band FM

(Continued)



## CHAPTER V . CONCLUSIONS

We have described the detector of Figure 1-6, which is inherently of low delay, excellent sensitivity, wide bandwidth, extremely linear, and ease of digital implementation. The low delay was obtained through the use of 1) networks having zero group delay, and 2) an RF cancellation technique for the carrier.

The theoretical performance of the detector obtained by Klapper, Kratt, and Tarbell was analyzed for the modulated input signals, unmodulated interference carriers, and narrow-band noises (CHAPTER 2). For interference signal levels approaching the desired signal level, the new detector has shown to offer a considerable improvement over the conventional limiter-discriminator detector. The noise performance was shown to be comparable to the conventional detector when it operates well above the threshold level. However, the threshold point had no improvement. These results were also compared with the other versions of Klapper-Kratt detectors, which showed improved performance in the areas of linearity, noise and threshold.

The digital implementation of the new detector was realized using FIR digital signal processing methods. And the results were then optimized for linearity.

Based on these results, the detector was realized using the digital signal processor INTEL-2920.

This means a laboratory model FM detector whose characteristics were comparable to the conventional limiter-discriminator FM detector when it operates well above the threshold region, was realized using only a single-chip DSP without introducing limiter and LPF for noise reduction and eliminating RF frequency. From the property of the INTEL-2920 DSP chip, which can handle digital output as well as analog output, the new FM detector may be useful for some other applications, for example, a low bit rate binary FM detector.

Referring to Kratt (Ref. 2), the performances of the two cases were observed and compared, which showed that the two systems had almost identical properties except the speed of the two systems.

#### References - Chapter 5.

1. INTEL, "The 2920 Analog Signal Processor Design Handbook," Intel Cor. August 1980.
2. E. Kratt, Optimization of a New Linear FM Detector Using Digital Signal Processing Techniques, Chapter 6. NJIT, Oct. 1982

## BIBLIOGRAPHY

### BOOKS

1. K. K. Clarke and D. T. Hess , Communications Circuits: Analysis and Design, Addison-Wesley, 1971
2. P. F. Panter, Modulation, Noise, and Spectral Analysis, Chapter 14, McGraw Hill, 1965.
3. M. Schwartz, Information Transmission, Modulation, and Noise, Chapter 6, McGraw Hill, 1970.
4. J. Klapper and J. T. Frankle, Phase Locked and Frequency Feedback Systems, Chapter 7, Academic Press, 1972.
5. S. D. Stearns, Digital Signal Analysis, Chapter 4, Hayden, 1975.
6. W. D. Stanley, G. R. Dougherty, and R. Dougherty, Digital Signal Processing, Chapter 15, Reston, 1984.
7. 2920 Analog Signal Processor Design Handbook, Chapter. 3, Intel Cor., 1980.

### PAPERS

1. E. Kratt and J. Klapper, "A New Digital Detector for Frequency Modulated Wave," 27<sup>th</sup> Midwest Symposium on Circuits and Systems, Morgantown, WV., June 1984.
2. J. Klapper and E. Kratt, "A New Family of Low-Delay FM Detectors," IEEE Transactions on Communications, Vol. COM-27, No. 2, Feb. 1979.

3. E. Kratt, "Optimization of a New Linear FM Detector Using Digital Signal Processing Techniques," A Doctoral Dissertation, NJIT, October, 1982.
4. J. Park, "An FM Detector for Low S/N," IEEE Transactions on Communication Technology, Vol. COM-18, No. 2, April, 1970
5. G. J. Kersus, "Analysis of the Klapper-Kratt FM Detector," M. S. Project, Dept. of Elec. Eng., NJIT., 1976.
6. M. S. Corrington, "Frequency Modulation Caused by Common-and-Adjacent-Channel Interference," RCA Rev. Vol. 7, Dec. 1946.
7. A. Tarbell and J. Klapper, "Noise Performance of the Klapper-Kratt Low Delay FM Detector," NTC, Washington, D.C., Nov. 1979.
8. J. H. McClellan, T. W. Parks and L. R. Rabiner, "FIR Linear Phase Filter Design Program," Programs for Digital Signal Processing, Chapter 5., IEEE Press, New York, 1979.
9. R. Fletcher and M. J. D. Powell, "A Rapidly Convergent Descent Method for Minimization," Computer J., Vol. 6, No. 2, July 1963.